MNRAS **000**, 1–25 (2015) Preprint April 5, 2016 Compiled using MNRAS LATEX style file v3.0

The bolometric light curves and physical parameters of stripped-envelope supernovae

S. J. Prentice[1⋆], P. A. Mazzali[1,2], E. Pian[3,4], A. Gal-Yam[5], S. R. Kulkarni[6], A. Rubin[5], A. Corsi[7], C. Fremling[8], J. Sollerman[8], O. Yaron[5], I. Arcavi[9,10], W. Zheng[11], M. M. Kasliwal[6,12], A. V. Filippenko[11], S. B. Cenko[13], Y. Cao[6], P. E. Nugent[14,11]

[1] *Astrophysics Research Institute, Liverpool John Moores University, IC2, Liverpool Science Park, 146 Brownlow Hill, Liverpool L3 5RF, UK*
[2] *Max-Planck-Institut für Astrophysik, Karl-Schwarzschild-Str. 1, D-85748 Garching, Germany*
[3] *Institute of Space Astrophysics and Cosmic Physics, via P. Gobetti 101, I-40129 Bologna, Italy*
[4] *Scuola Normale Superiore, Piazza dei Cavalieri 7, I-56126 Pisa, Italy*
[5] *Department of Particle Physics and Astrophysics, Weizmann Institute of Science, 76100 Rehovot, Israel*
[6] *Division of Physics, Mathematics, and Astronomy, California Institute of Technology, 1200 E California Blvd., Pasadena, CA 91125, USA*
[7] *Texas Tech University, Physics Department, Box 41051, Lubbock, TX 79409-1051, USA*
[8] *The Oskar Klein Centre, Department of Astronomy, Stockholm University, 10691 Stockholm, Sweden*
[9] *Las Cumbres Observatory Global Telescope Network, 6740 Cortona Dr, Suite 102, Goleta, CA 93111, USA*
[10] *Kavli Institute for Theoretical Physics, University of California, Santa Barbara, CA 93106, USA*
[11] *Department of Astronomy, University of California, Berkeley, CA 94720-3411, USA*
[12] *The Observatories, Carnegie Institution for Science, 813 Santa Barbara st, Pasadena, CA 91101, USA*
[13] *Astrophysics Science Division, NASA Goddard Space Flight Center, Mail Code 661, Greenbelt, MD 20771, USA*
[14] *Lawrence Berkeley National Laboratory, 1 Cyclotron Rd., Berkeley, CA 94720, USA*

Accepted XXX. Received YYY; in original form ZZZ

ABSTRACT

The optical and optical/near-infrared pseudobolometric light curves of 85 stripped-envelope supernovae (SNe) are constructed using a consistent method and a standard cosmology. The light curves are analysed to derive temporal characteristics and peak luminosity $L_{\rm p}$, enabling the construction of a luminosity function. Subsequently, the mass of ^{56}Ni synthesised in the explosion, along with the ratio of ejecta mass to ejecta kinetic energy, are found. Analysis shows that host-galaxy extinction is an important factor in accurately determining luminosity values as it is significantly greater than Galactic extinction in most cases. It is found that broad-lined SNe Ic (SNe Ic-BL) and gamma-ray burst SNe are the most luminous subtypes with a combined median $L_{\rm p}$, in erg s^{-1}, of $\log(L_{\rm p}) = 43.00$ compared to 42.51 for SNe Ic, 42.50 for SNe Ib, and 42.36 for SNe IIb. It is also found that SNe Ic-BL synthesise approximately twice the amount of ^{56}Ni compared with SNe Ic, Ib, and IIb, with median $M_{\rm Ni} = 0.34$, 0.16, 0.14, and 0.11 M$_\odot$, respectively. SNe Ic-BL, and to a lesser extent SNe Ic, typically rise from $L_{\rm p}/2$ to $L_{\rm p}$ more quickly than SNe Ib/IIb; consequently, their light curves are not as broad.

Key words: supernovae: general

1 INTRODUCTION

Stars with zero-age main sequence (ZAMS) mass $\gtrsim 8$ M$_\odot$ have short lives that end with the catastrophic gravitational collapse of the stellar core (e.g., Smartt 2009). The structure of the resulting electromagnetic emission observed due to the explosion depends upon the evolution of the progenitor star. It is possible for the star to be stripped of its outer envelope by either strong winds during the Wolf-Rayet phase (e.g., Gal-Yam et al. 2014; Smith & Owocki 2006), interaction with a binary companion (e.g., Eldridge et al. 2013), or some combination of the two. The result is an absence of H in the spectra, which characterises Type Ib/c supernovae (SNe Ib, SNe Ic). If the envelope stripping is highly

⋆ E-mail: S.J.Prentice@2014.ljmu.ac.uk

efficient, then the He shell is removed as well, and it is the presence or absence of He which differentiates between Type Ib and Type Ic SNe, respectively. (For extensive reviews of the optical spectra of SNe Ib and Ic, see Filippenko 1997 and Matheson et al. 2001.) In addition, some SNe show H lines around maximum light which rapidly disappear (Filippenko 1988; Filippenko et al. 1993). They are canonically classified as Type IIb SNe (e.g., Nomoto et al. 1993) but are included here, along with SNe Ib/c, in the broader category of stripped-envelope supernovae (SE-SNe; Filippenko 1997; Clocchiatti & Wheeler 1997).

SE-SNe are typically characterised by heterogeneous light-curve (LC) shapes, and luminosities where the LC $M_{\rm peak}$ is typically between -16 mag and -18.5 mag. The decay of ^{56}Ni to ^{56}Co, and then to ^{56}Fe, powers the light curve (Tominaga et al. 2005) in the vast majority of cases. A notable exception to this is the magnetar powered SN 2011kl associated with the ultralong gamma-ray burst (GRB) 111209A (Greiner et al. 2015). The spectra of SE-SNe show photospheric velocities ($v_{\rm ph}$) ranging between $\sim$ 5000 km s^{-1} and 25,000 km s^{-1} at maximum light. A significant amount of ejecta at higher velocities, $\gtrsim 18,000$ km s^{-1}, results in broad absorption lines that led to significant line blending in the spectra and reduces the number of visible features. SNe with high $v_{\rm ph}$ are almost exclusively Type Ic; for exceptions, see the Type IIb SN 2003bg (Hamuy et al. 2009) and the Type IIn SN 1997cy (Turatto et al. 2000). They possess kinetic energies $E_{\rm k} > 10^{52}$ erg, an order of magnitude greater than typical SE-SNe. SNe with $E_{\rm k}$ in this extreme range have sometimes been labeled "hypernovae" (HNe; Iwamoto et al. 1998). Type Ic HNe form a subpopulation known as broad-lined SNe Ic (SNe Ic-BL; e.g., SN 2002ap, SN 1997ef; Mazzali et al. 2002, 2000).

Since 1998, some SNe Ic have been associated with GRBs when SN 1998bw was discovered in the error box of GRB 980425 (Galama et al. 1998). The GRB/SN connection was later confirmed by the spectroscopic association of SN 2003dh with GRB 030329 (e.g., Matheson et al. 2003; Hjorth et al. 2003). To date, more than two dozen GRB-SNe have been discovered, either photometrically or spectroscopically. Of those SNe that are spectroscopically confirmed, all are Type Ic HNe showing characteristic broad lines in their spectra. In addition, the Type Ib SN 2008D (Mazzali et al. 2008; Soderberg et al. 2008) was associated with the weak X-ray flash (XRF) 080109. The energetics of the GRBs associated with SNe are varied. It was initially thought that these GRBs represented a different population as they were often underluminous in γ-rays. With more data, it was found that luminosities in this photon range were typical but showed variations of a few orders of magnitude. For example, GRB 060218 associated with SN 2006aj is more commonly considered to be an XRF given the low γ-ray luminosity. The diversity of GRB energetics associated with the GRB SNe has implications for the progenitor stars and the powering mechanism of the SN itself. It is unfortunate that observational circumstances, such as distance and competition with the GRB afterglow, conspire to make GRB-SNe generally difficult to observe. However, their unambiguous explosion dates make them an important baseline for this study.

There have been attempts in the last few years to investigate the bulk properties of core-collapse SNe. Cano (2013) presented a method of estimating explosion properties of 61 SNe Ib/c using SN 1998bw as a template. Taddia et al. (2015) used data from the Sloan Digital Sky Survey SN survey II (SDSS-II) to build a set of 20 SN Ib/c bolometric light curves and their corresponding properties. Drout et al. (2011) took 25 SNe Ibc/II and used multiband light curves, as well as taking R-band data as a proxy for the bolometric emission, to estimate the characteristics of the SNe. Pritchard et al. (2014) used *Swift* data to build bolometric light curves for core-collapse SNe but were limited to a redward limit of the *Swift*-UVOT V band. Lyman et al. (2016) utilised a method of deriving bolometric values for 38 SNe from colours. However, as yet no single study of the individually derived bulk properties of SE-SNe found within the literature has been published. Motivated by this gap, the aims of this study are to build a self-consistent set of bolometric light curves using the available photometry, investigate the derived explosion parameters, determine the temporal characteristics of each SN, and compare with the light curves of multiband photometry.

2 DATABASE

We compiled a list of data for SE-SNe which are publicly available in the literature. Over 100 were found, typically covering a period of $\sim$ 20 years. In most cases, the data were found in studies involving single objects. However, larger datasets have recently been published. Bianco et al. (2014) presented 64 SNe Ib/c observed by the Harvard-Smithsonian Center for Astrophysics (CfA) SN group in the period 2001 to 2009. 20 SNe Ib/c from the SDSS-II were analysed by Taddia et al. (2015) using data from Sako et al. (2014). Consequently, the number of SNe available more than doubled in less than a year. In addition to this, we gained access to the Palomar Transient Factory (PTF)[1] (Law et al. 2009) and the intermediate Palomar Transient Factory (iPTF) archives, increasing the number of SNe available. Thus, the total number of SNe in the initial database is as follows:

- Public — single object — $\sim$ 50
- Public — CfA — 64
- Public — SDSS II — 20
- Public — *Swift* — 15
- iPTF/PTF — 128.

2.1 Selection criteria

With a large database of SNe, the next step was to consider what was required from the dataset. To build a consistent group of bolometric LCs it was necessary that, as best as possible, the photometry from SN to SN was well sampled over the same rest-frame wavelength range. Ideally, the sample should have shown good coverage in the wavelength range corresponding to the bulk of the SN light (i.e., between the V and R bands), which also corresponds to the turnover in the spectral energy distribution (SED) around bolometric peak. It should also have sufficient coverage in adjacent bands in order to build SEDs across a uniform wavelength range and, as we wanted to derive time-dependent parameters from the SN peak, it was essential that the coverage

[1] www.ptf.caltech.edu

included this epoch. This led to the following two criteria for inclusion in our sample:

- The peak of the SN must be observed in the BVR bands or equivalents.
- The temporal coverage must have been sufficient that the rise and/or decay time from half-maximum luminosity to maximum luminosity could be derived or the explosion date well constrained.

These restrictions immediately ruled out more than 70% of the literature SNe, with the majority lacking observations at peak or sufficient coverage in multiple filters. This affected the CfA and *Swift* set considerably. Only half of the CfA sample showed a clear photometric peak, and for SNe observed solely by *Swift* the lack of observations redward of the UVOT V band means that the peak of the SED, and hence the bulk of the light, was missed in every case. Of the PTF/iPTF SNe, most had to be rejected because they were observed only in the r band.

Table 1 lists the 85 SNe that fulfilled the criteria. The sample consists of 25 SNe Ib, 21 SNe Ic, 12 SNe Ic-BL, 10 GRB-SNe, 15 SNe IIb, and 2 SNe Ibc. (The SNe Ibc have an ambiguous classification; the data were not of sufficient quality to distinguish between the Ib and Ic subclasses.) SNe with full optical and near-infrared (NIR) coverage allowed the construction of an effective bolometric light curve as opposed to a pseudobolometric optical variant.

3 CONSTRUCTING THE BOLOMETRIC LIGHT CURVE

3.1 Missing data

In order to derive the bolometric luminosity of a SN at a particular date, an SED constructed from the photometry is required. Thus, it was essential that there was photometry in the relevant bands at that time, which was not always the case. In order to attain temporal uniformity, the worst-sampled band was chosen to be a reference point and the remaining bands were fit with a linear spline. The magnitudes were interpolated on the dates of the reference band. Early-time data points are especially important as they help determine the rise time of the SN and constrain t_0, the time of explosion. However, these epochs also tended to be sparsely sampled, often with observations in just a couple of bands.

To obtain estimates of the early-time bolometric data points, two methods were used to extrapolate missing photometry provided that at least two bands were available and one of them was a V-band equivalent (e.g., an effective wavelength around 4000–5000 Å). If the temporal gap between the first date in two adjacent bands was no greater than a few days, then either a constant colour was assumed or the mean colour evolution of similar SN types was adopted. If it was not possible to use this method, but there were sufficient pre-peak data, then extrapolations were done via a low-order polynomial fit to the data. As per the previous method, this technique was limited to time periods on the order of a few days. Care was taken to avoid extrapolating early-time data points based upon the behaviour of the light curves near peak, as this would have underestimated the rate of change. Given the uncertain nature of the shape of the light curve outside the observed dates, large errors of ~ 1 mag on the extrapolations were assumed.

3.2 GRB-SNe and afterglow subtraction

The desire to include as many GRB-SNe as possible in the database is compromised by the difficulty in deconvolving the SN light from that of the GRB afterglow and host galaxy. For some SNe (e.g., SN 1998bw), the afterglow is negligible, so optical emission is dominated by SN photons; however, this is not usually the case. To calculate the afterglow component of the light curve, the spectrum is considered to follow a simple relation given by $F_\nu(t,\nu) \propto t^{-\alpha}\nu^{-\beta}$. We defer to the literature for the numerical values of the temporal and spectral indices and subtract the afterglow flux from the SEDs as required. Additionally, it is common in the literature to fit the afterglow-SN-host light curve with a template SN based on SN 1998bw (Cano 2013), but this method is not adopted here to avoid biasing any temporal characteristics that may be extracted from the light curve.

There are approximately 20 GRB-SNe given in the literature. Most are photometrically associated with the GRB (e.g., they show a late-time bump in the light curve), but unfortunately the majority of these are poorly observed, with few data points in only a few bands and showing large afterglow contamination. Consequently, the number of usable GRB-SNe is greatly restricted. It is an unfortunate irony that GRB-SNe in general have the best-known explosion date yet the most poorly constrained photometry.

3.2.1 SN 2003dh / GRB 030329

To form as complete a sample as possible, the light curve of SN 2003dh from Deng et al. (2005) is included in the database. The ultraviolet-optical-infrared (UVOIR) light curve is the result of synthetic photometry from spectra and a mean bolometric correction, derived from SN 1998bw, added to the photometric data. A consequence of this is that we do not desconstruct the light curve to obtain a $BVRI$ variant and use the data as is.

3.3 Distance

A primary goal of this study was to present a self-consistent set of bolometric light curves. In order to achieve this, it was necessary (where possible) to obtain a distance modulus for each SN adopting a standard cosmological model. Thus, the distance modulus of each SN was taken from the NASA/IPAC Extragalactic Database (NED)[2] for the host galaxy using the standard NED cosmological model ($H_0 = 73.0$ km s^{-1} Mpc^{-1}, $\Omega_m = 0.27$, $\Omega_\Lambda = 0.73$) and corrected for Galactic motion toward Virgo, the Great Attractor, and the Shapley Supercluster. The standard uncertainty of 0.15 mag in the NED values was adopted throughout.

Figure 1 shows the redshift distribution of SNe within the database. 88% lie at $z < 0.1$, with the median being $z = 0.0189$. Statistics for the redshift distribution by spectral type are given in Table 2

[2] https://ned.ipac.caltech.edu/

Table 1. The database of 85 SNe included in this work.

SN	Type	μ (mag)	z	$E(B-V)_{\rm MW}$ (mag)	$E(B-V)_{\rm host}$ (mag)	references
1993J	IIb	27.8	-0.000113	0.071	0.1	(1)
1994I	Ic	29.6	0.0015	0.03	0.3	(2)
1996cb	IIb	29.95	0.0024	0.12	negligible	(3)
1998bw	GRB-SN	32.76	0.0087	0.052	negligible	(4),(5)
1999dn	Ib	32.93	0.0093	0.052	0.1	(6)
1999ex	Ib	33.44	0.0114	0.02	0.28	(7)
2002ap	Ic-BL	29.5	0.0022	0.071	0.008	(8),(9),(10)
2003bg	IIb	31.68	0.0046	0.02	negligible	(11)
2003dh	GRB-SN	39.21	0.168	0.025	negligible	(12)
2003jd	Ic-BL	34.43	0.019	0.06	0.09	(13)
2004aw	Ic	34.31	0.016	0.021	0.35	(14)
2004fe	Ic	34.28	0.018	0.0210	-	(15)
2004gq	Ib	32.09	0.0065	0.0627	0.095	(15)
2005az	Ic	33.14	0.0085	0.0097	-	(15)
2005bf	Ib	34.62	0.019	0.045	negligible	(16)
2005hg	Ib	34.68	0.021	0.0901	-	(15)
2005hl	Ib	34.92	0.023	0.073	-	(17)
2005hm	Ib	35.85	0.035	0.048	-	(17)
2005kl	Ic	31.64	0.0035	0.0219	-	(15)
2005kr	Ic-BL	38.91	0.134	0.087	-	(17)
2005ks	Ic-BL	38.21	0.099	0.05	-	(17)
2005kz	Ic	35.31	0.027	0.046	-	(15)
2005mf	Ic	35.27	0.027	0.0153	-	(15)
2006T	IIb	32.68	0.0080	0.0647	-	(15)
2006aj	GRB-SN	35.61	0.033	0.097	negligible	(18),(19),(20)
2006el	IIb	34.25	0.017	0.0973	-	(15)
2006ep	Ib	33.93	0.015	0.036	-	(15)
2006fe	Ic	37.41	0.07	0.098	-	(17)
2006fo	Ib	34.58	0.021	0.025	-	(15)
14475[a]	Ic-BL	39.17	0.149	0.072	-	(17)
2006jo	Ib	37.63	0.077	0.032	-	(17)
2006lc	Ib	34.13	0.016	0.057	-	(17)
2006nx	Ic-BL	38.97	0.137	0.108	-	(17)
2007C	Ib	32.15	0.0059	0.0363	0.73	(15)
2007D	Ic-BL	34.84	0.023	0.2881	-	(15)
2007Y	Ib	31.29	0.0046	0.022	0.09	(24)
2007ag	Ib	34.78	0.020	0.025	-	(15)
2007cl	Ic	34.84	0.022	0.02	-	(15)
2007gr	Ic	29.84	0.0017	0.055	0.03	(21)
2007kj	Ib	34.3	0.018	0.0691	-	(15)
2007ms	Ic	36.09	0.039	0.184	-	(17)
2007nc	Ib	37.91	0.087	0.025	-	(17)
2007qv	Ic	38.11	0.095	0.048	-	(17)
2007qx	Ic	37.71	0.08	0.023	-	(17)
2007ru	Ic-BL	34.04	0.016	0.27	negligible	(22)
2007sj	Ic	36.09	0.039	0.032	-	(17)
2007uy	Ib	32.48	0.0065	0.022	0.63	(23)
2008D	Ib	32.48	0.0065	0.02	0.63	(27),(15),(28)
2008ax	IIb	29.82	0.0019	0.022	0.278	(25),(26)
2008bo	IIb	32.06	0.005	0.0513	0.0325	(15)
2008hw	GRB-SN	42.35	0.53	0.42	negligible	(15)
2009bb	Ic	33	0.00988	0.098	0.482	(29)
2009er	Ib	35.9	0.035	0.0389	-	(15)
2009iz	Ib	33.8	0.014	0.0729	-	(15)
2009jf	Ib	32.64	0.0079	0.112	0.05	(30)
2010as	IIb	32.17	0.0073	0.15	0.42	(31)
2010bh	GRB-SN	36.94	0.059	0.12	0.14	(32)
2010ma	GRB-SN	42.40	0.552	0.019	0.04	(32)
2011bm	Ic	34.95	0.022	0.032	0.032	(33)
2011dh	IIb	29.48	0.0020	0.035	0.05	(34)
2011ei	IIb	33.09	0.0093	0.059	0.18	(35)
2011fu	IIb	34.36	0.019	0.068	0.015	(36)
2011hs	IIb	31.91	0.0057	0.011	0.16	(37)
2011kl	GRB-SN	43.09	0.677	0.019	0.038	(38)

Table 1 – *continued* The database of 85 SNe included in this work

SN	Type	μ (mag)	z	$E(B-V)_{\rm MW}$ (mag)	$E(B-V)_{\rm host}$ (mag)	references
2012ap	Ic-BL	33.45	0.012	0.045	0.4	(39)
2012bz	GRB-SN	40.31	0.28	0.037	negligible	(40)
2013cq	GRB-SN	41.19	0.34	0.02	0.05	(41)
2013cu	IIb	35.23	0.026	0.011	negligible	(42)
2013df	IIb	31.65	0.0024	0.017	0.08	(43)
2013dx	GRB-SN	39.04	0.145	0.04	0.10	(44)
2013ge	Ibc	31.87	0.0044	0.02	0.047	(45)
PTF09dh/2009dr[b]	Ic-BL	37.60	0.076	0.022	-	-
PTF10gvb	Ic-BL	38.26	0.098	0.022	-	-
PTF10inj	Ib	37.31	0.066	0.01	-	-
PTF10qif	Ib	37.26	0.064	0.0587	-	-
PTF10vgv	Ic	34.01	0.015	0.145	-	(49)
PTF11bli	Ibc	35.81	0.034	0.013	-	-
PTF11jgj	Ic	36.15	0.04	0.027	-	-
PTF11klg	Ic	35.26	0.027	0.03	-	-
PTF11qiq	Ib	35.66	0.032	0.066	-	-
PTF11rka	Ic	37.61	0.074	0.03	-	-
PTF12gzk	Ic	33.8	0.014	0.14	negligible	(48)
PTF12os	IIb	31.89	0.0045	0.045	-	(50)
iPTF13bvn	Ib	31.89	0.0045	0.0278	0.0437	(46),(47)
iPTF14dby	Ic-BL	37.54	0.074	0.048	-	(51)

References: (1) Richmond et al. (1994), (2) Richmond et al. (1996), (3) Qiu et al. (1999), (4) Clocchiatti et al. (2011), (5) Patat et al. (2001), (6) Benetti et al. (2011), (7) Stritzinger et al. (2002), (8) Foley et al. (2003), (9) Gal-Yam et al. (2002), (10) Tomita et al. (2006), (11) Hamuy et al. (2009), (12) Deng et al. (2005), (13) Valenti et al. (2008), (14) Taubenberger et al. (2006), (15) Bianco et al. (2014), (16) Anupama et al. (2005), (17) Taddia et al. (2015), (18) Pian et al. (2006),(19) Mirabal et al. (2006), (20) Kocevski et al. (2007), (21) Hunter et al. (2009), (22) Sahu et al. (2009), (23) Roy et al. (2013), (24) Stritzinger et al. (2009), (25) Pastorello et al. (2008), (26) Taubenberger et al. (2011), (27) Mazzali et al. (2008), (28) Modjaz et al. (2009), (29) Pignata et al. (2011), (30) Valenti et al. (2011), (31) Folatelli et al. (2014), (32) Bufano et al. (2012), (33) Valenti et al. (2012), (34) Marion et al. (2014), (35) Milisavljevic et al. (2013), (36) Kumar et al. (2013), (37) Bufano et al. (2014), (38) Greiner et al. (2015), (39) Milisavljevic et al. (2015), (40) Melandri et al. (2012), (41) Melandri et al. (2014), (42) Gal-Yam et al. (2014), (43) Morales-Garoffolo et al. (2014), (44) D'Elia et al. (2015), (45) Drout et al. (2015), (46) Fremling et al. (2014), (47) Srivastav et al. (2014), (48) Ben-Ami et al. (2012), (49) Corsi et al. (2012), (50) Fremling et al. (2016, in prep.), (51) Corsi et al. (2016, in prep.).
[a]SN 14475 was discovered in 2006 as part of the SDSS-II SN survey.
[b]PTF09dh/SN 2009dr was originally classified at a Type Ia SN but later reclassified as a Ic-BL.

Table 2. Redshift statistics of sample SNe by spectral type

Type	median z	mean z	range	Number
GRB-SNe	0.224	0.279	0.0087–0.677	10
Ic-BL	0.075	0.069	0.0022–0.149	12
Ic	0.022	0.031	0.0015–0.095	21
Ibc	0.019	0.019	0.0044–0.034	2
Ib	0.018	0.025	0.0045–0.087	25
IIb	0.0050	0.0076	< 0.0258	15

3.4 Extinction

Extinction values were taken from the literature, and the reddening correction was done using the extinction law given by Cardelli et al. (1989). However, it was apparent that not all SNe have spectroscopically derived host-galaxy extinction, an issue which affects half the SNe used here. We find that in cases where both extinction values are known, the database has a mean $E(B-V)_{\rm MW} = 0.059$ mag, significantly less than the mean host-galaxy extinction of $E(B-V)_{\rm host} = 0.135$ mag. Thus, failure to include the effect of host reddening results in less-luminous bolometric LCs for those SNe and places the values derived as lower limits.

It is desirable to make as few assumptions as possible while constructing the set of bolometric light curves. However, it is acknowledged that taking the host-galaxy reddening to be zero for some SNe and then attempting to include them in population statistics biases the sample by selecting a value at a boundary of a distribution. We also want to maximise the number of SNe in the sample, so we adopt the following procedure. When calculating the properties of individual SNe, no correction was made when the host extinction was unknown. The values derived are taken as lower limits in this case. For the bulk sample we dereddened the flux for a median host extinction of that SN type. This works on the basis that the extinction would be typically around the mean and the number of SNe overcorrected would balance the number of SNe undercorrected. This increases the spread of the distribution but provides a better estimate of the median and mean than using lower limits.

To examine this in more detail, we searched the liter-

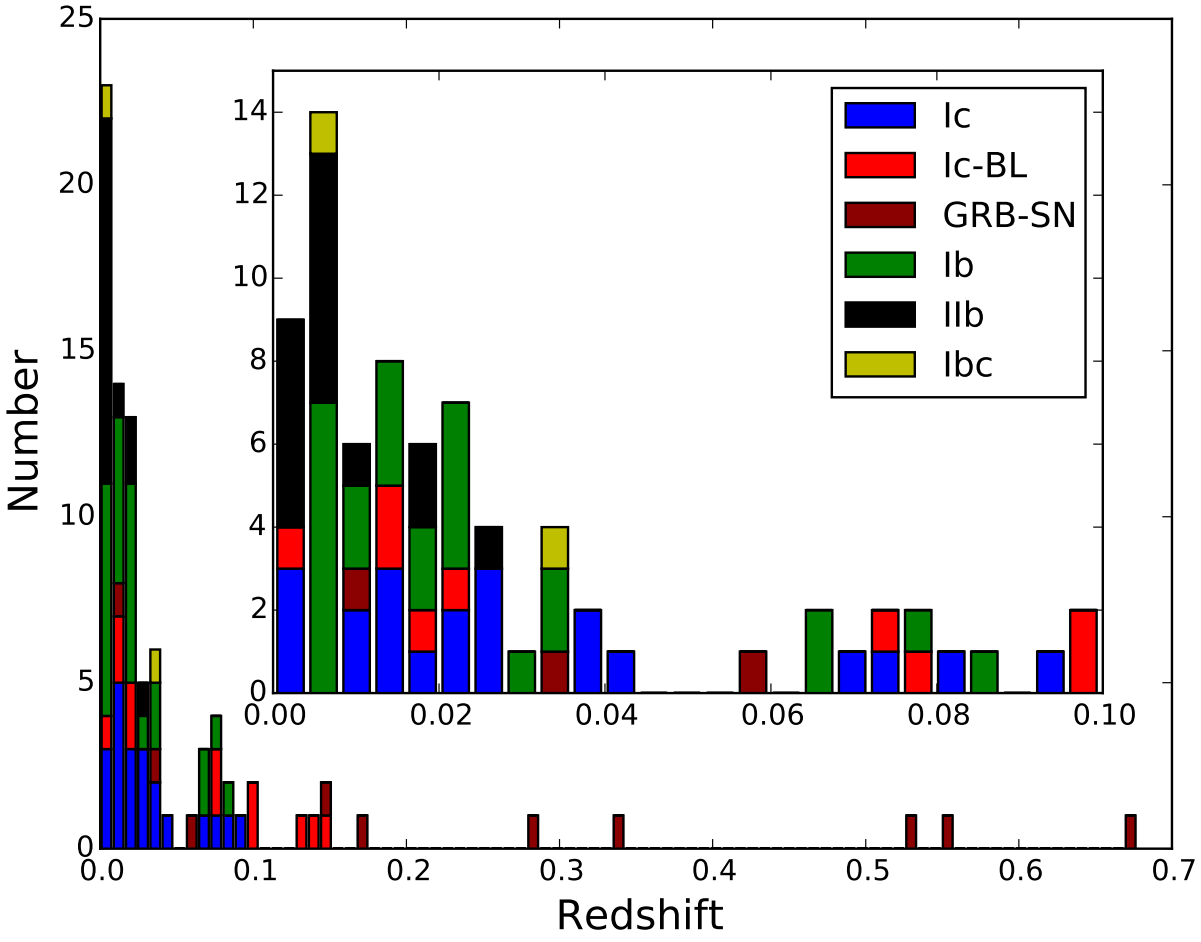

Figure 1. Redshift distribution of the SNe in the sample. The vast majority of SNe are found at $z < 0.1$, as demonstrated in the inset. It is clear that the high-z regime is dominated by GRB-SNe.

ature for core-collapse SNe, including all SNe II, and built a set of host-galaxy extinction functions by type. The host galaxies of observed GRB-SNe are known to be different from those of other core-collapse SNe in terms of metallicity (e.g., Modjaz et al. 2008; Graham & Fruchter 2013) — so if the extinction is dependent on host, host inclination, and SN type, then the distributions should reflect this. The results of this work are presented in the Appendix, with the results given in Table A1.

Finally, we note that only the spectroscopically derived host-galaxy extinction, such as from the equivalent width of Na I D absorption lines (Poznanski et al. 2012), is used here.

3.5 Constructing the SED

To construct the SED the photometry was corrected for Galactic extinction in the observer frame and, if possible, corrected for host extinction in the rest frame. Uncertainties in reddening were included in quadrature. When the monochromatic flux, calculated from the photometry (see Bessell et al. 1998; Fukugita et al. 1995), was shifted to the rest frame wavelength it was also multiplied by $(1+z)$, which is a useful approximation in the absence of spectroscopically derived K-corrections. The process of flux conversion depends upon the filter system used. Data in the literature cover more than twenty years of observations and over this period there has been a shift in the usage of filters from Johnson-Cousins (J-C) *UBVRIJHK* (and minor variations) to SDSS type filters ($u'g'r'i'z'$) or some combination of these, as well as space telescope specific filters such as those on the *Swift*-UVOT. The two main standards use different flux units with the J-C system being based on Vega and SDSS on AB. As default all SEDs are constructed in units of erg s^{-1} cm^{-2} $^{-1}$. This required conversion of the SDSS filters which was achieved by using the relation $\lambda f_\lambda = \nu f_\nu$.

The rest frame flux was fit with a linear spline to create SEDs over the range 3000 to 10000 for *UBVRI*-equivalents, 4000 to 10000 for *BVRI*-equivalents, and 10000 to 24000 for NIR.

Table 3. SED integration wavelength range and terminology.

Constituent bands	Wavelength range (Å)	Nomenclature
$BVRI/g'r'i'z'$	4000–10,000	$BVRI$
$UBVRI/u'g'r'i'z'$	3000–10,000	$UBVRI$
JHK	10,000–24,000	NIR

3.6 From SED to pseudobolometric luminosity

The rest-frame SEDs were then integrated over the wavelength range, assuming zero flux outside the limits. The effect due to redshift and the subsequent blueshifting of the effective wavelengths of the photometry is small (a few percent) out to $z \approx 0.1$. Beyond this, the bluest bands start to be shifted outside the integration range and the reddest effective wavelength shifts to a more central position; in this regime, the largest uncertainty comes from the behaviour of the tail of the SED. If there is photometry in bands with effective wavelengths longer than I/i', we incorporate these into the optical SEDs, as they are blueshifted into the optical wavelength range or close to it.

We note that one might be tempted to fit a blackbody emission curve to the SEDs, but this is erroneous as the spectrum of a SN is not a blackbody. During the photospheric phase, the UV suffers line blanketing, the severity of which is related to the amount of iron-group elements (Mazzali 2000) and the velocity of the ejecta, which causes line broadening. The photons scattered in this process eventually escape at redder wavelengths creating a flux excess at these points (e.g., Mazzali & Lucy 1993). In the nebular phase (> 60 days), the spectrum is dominated by line emission as the optically thin ejecta are excited via energy deposition from the γ-rays and positrons emitted during the decay of ^{56}Ni to ^{56}Fe (Mazzali et al. 2005).

The uncertainties were carried through the integration by evaluating the integral at the upper and lower errors of the flux. Once the bolometric flux was determined it was converted to bolometric luminosity using the distance.

4 PSEUDOBOLOMETRIC LIGHT CURVES

In order to compare bolometric light curves effectively, a set of $BVRI$, $UBVRI$, and NIR (or equivalent) LCs were produced, where the data allowed. Table 3 lists the bands, total wavelength range, and reference name throughout the paper for the different light curves. Within the sample, 84 SNe have a $BVRI$ LC, 44 have a $UBVRI$ LC, and 24 have a NIR LC. Various extensions of the LCs can be made by combining the data (e.g., $UBVRI$NIR). In most cases, the NIR is less well sampled than the optical, so to construct an optical-NIR LC the ratio between the two datasets was calculated for coincident dates. This was subsequently fit with a linear spline, and the NIR flux was deduced by interpolation of the ratio and the value of the optical flux on the dates when NIR observations were absent. When the optical LC extended beyond the NIR, the flux ratio was kept constant beyond the boundaries.

Finally, the temporal evolution of the light curve was corrected to the rest frame and set with a fiducial $t(0)$ at the time of maximum luminosity with the following caveat:

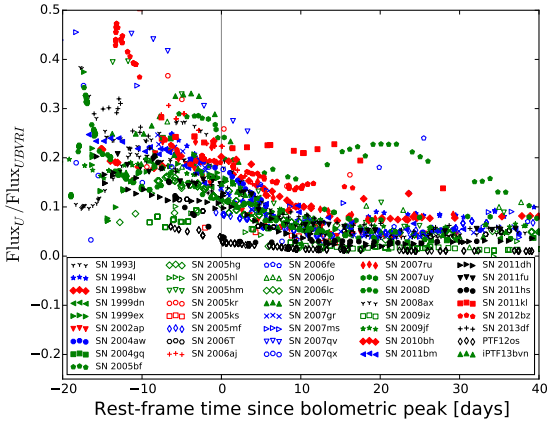

Figure 2. The ratio of the U/u'-band flux to the $UBVRI$ flux as a function of time. Open symbols represent SNe that have not had host-galaxy extinction corrections applied. The high host extinction of PTF12os is apparent in this diagram as the U/u' flux is negligible. The temporal evolution of peculiar SN Ib 2005bf is a noteworthy feature

any peak caused by early-time shock breakout (e.g., SN IIb 2013df Van Dyk et al. 2014) is ignored, and the later peak powered by radioactive decay is selected. In the case of peculiar SN Ib 2005bf, with its double-peaked light curve (Tominaga et al. 2005), we took the first peak to be the result of the decay of ^{56}Ni and the second peak a different energy-injection process, specifically a magnetar (Maeda et al. 2007). For a different interpretation, see Folatelli et al. (2006).

4.1 The contribution of U to $UBVRI$

Figure 2 gives the time-dependent contribution of the U/u'-band flux to the total $UBVRI$ flux. As expected, the SNe are bluer at earlier times than later. Table 4 shows the statistics for the sample at bolometric peak by spectral type and with/without host-extinction corrections applied. Note that the statistics are derived from two overlapping populations and there is a bias in the non-host-corrected SN Ic values caused by a few SNe with poorly constrained u' photometry. The SNe Ic-BL are demonstrably bluer at this epoch than other SN types with a U flux contribution of $\sim 20\%$ as opposed to $\sim 16\%$ for the other types (host-extinction correction included). We do note the small sample size in some cases.

4.2 NIR contribution

Figures 3 and 4 show the contribution of the NIR to the $BVRI$NIR and $UBVRI$NIR light curves, respectively. The median, mean, and standard-deviation statistics are given in Table 4. We have insufficient numbers to split the sample into subtypes, so we perform the analysis on all available SNe, regardless of whether there is a host-galaxy extinction value. We find that around peak, mean $\approx$ median, with a standard deviation of $\sim 4\%$ in both cases. It is possible that we have a bias in the sample given that the total number in each case is 18 and 12, which represents 21% and 14%

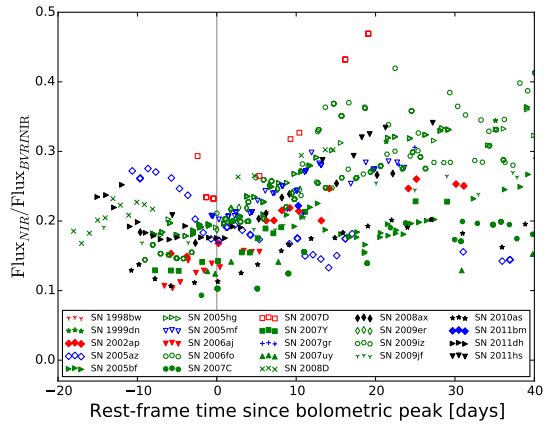

Figure 3. The ratio of NIR flux to *BVRI*NIR flux. Only dates when the optical and NIR observations were coincident are included.

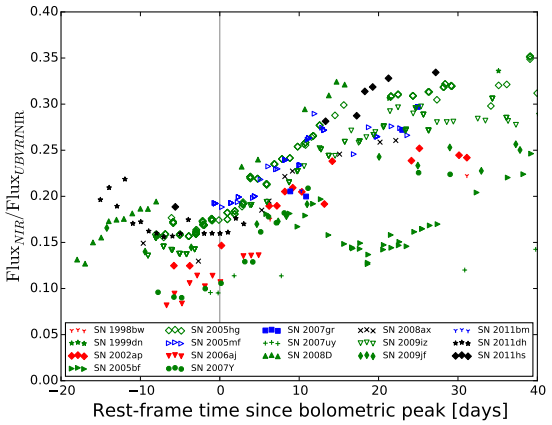

Figure 4. The ratio of NIR flux to *UBVRI*NIR flux. Only dates when the optical and NIR observations were coincident are included.

of the total database, respectively. To test the probability of the statistical values being returned by chance, we run a Monte-Carlo simulation in which we randomly place 85 SNe with a uniform distribution in a NIR/ONIR "box" of varying width. From this box, 18 SNe (12 for NIR/*UBVRI*NIR) are randomly selected and their bulk median/mean ratio and standard deviation measured. We define an acceptable parameter set as $0.9 <$ ratio < 1.1 and standard deviation < 0.4; there is no constraint on the values of median or mean, only their ratio. If the returned values fulfil these criteria then it is considered a hit. We perform 5000 runs for each window and return P(ratio) = hit/runs. The results are sensitive to the allowed variation in the ratio and the standard deviation, both of which we choose to be in excess of the measured values. We find that for NIR/*BVRI*NIR, a window of > 0.16 gives $P < 0.025$, while for NIR/*UBVRI*NIR, a window of > 0.18 gives $P < 0.064$. We conclude that the observed median and mean are not a sampling bias caused by too few SNe; they represent typical values.

The contribution of the NIR is generally small throughout with the exception of SN 2005kl, which was extremely red and has a NIR to optical ratio > 1; consequently, it has been omitted from Figure 3. Bianco et al. (2014) noted that this SN occurred in an H II region of NGC 4369, a galaxy with a high continuum gradient. They also do not attribute the red colour to high intrinsic extinction. Spectra of the object show that it is dominated by galactic emission and displays a red continuum. Accordingly, we do attribute the red colour to host-galaxy extinction. On this basis it has not been included in the process of determining the NIR flux fraction.

Table 4. Flux-ratio statistics at bolometric peak.

U-band contribution to *UBVRI* with host extinction			
Type	median	mean	standard deviation
SNe Ic-BL/GRB-SNe	0.20	0.20	0.03
SNe Ic	0.15	0.15	0.02
SNe Ib	0.16	0.20	0.05
SNe IIb	0.16	0.17	0.06
U-band contribution to *UBVRI* without host extinction			
Type	median	mean	standard deviation
SNe Ic-BL/GRB-SNe	0.18	0.19	0.07
SNe Ic	0.16	0.19	0.09
SNe Ib	0.13	0.15	0.07
SNe IIb	0.11	0.14	0.07
NIR contribution to optical/NIR			
Type	median	mean	standard deviation
NIR/*BVRI*NIR	0.17	0.17	0.04
NIR/*UBVRI*NIR	0.14	0.15	0.03

5 LIGHT-CURVE STATISTICS

5.1 Light curves

The *BVRI* LCs are shown by spectral type in Figures 5 and 6. The peak luminosity ranges from 5.6×10^{41} erg s^{-1} to $\sim 2.1 \times 10^{43}$ erg s^{-1}, a factor of ~ 100. Note that this range does not include PTF12os or SN 2005kl, both of which suffer from significant but unquantified host-galaxy extinction. 18 of the SNe available have sufficient photometry to be able to construct *UBVRI*NIR light curves. These SNe represent our "gold" sample and are shown in Figure 7. In some cases, the light curves are lower limits owing to the lack of information on host extinction.

The *BVRI* pseudobolometric light curves are shown en-masse in Figure 8. The final light curves will be uploaded to WISeREP[3] (Yaron & Gal-Yam 2012).

5.2 Luminosity functions

The luminosity function (see, for example, Li et al. 2011) for the *BVRI* sample, which includes those SNe where the median host-galaxy extinction has been included, is shown in Figure 9. Table 5 gives the statistics of the distribution. The collective SN Ic-BL/GRB-SN group is most luminous, and

[3] http://wiserep.weizmann.ac.il/

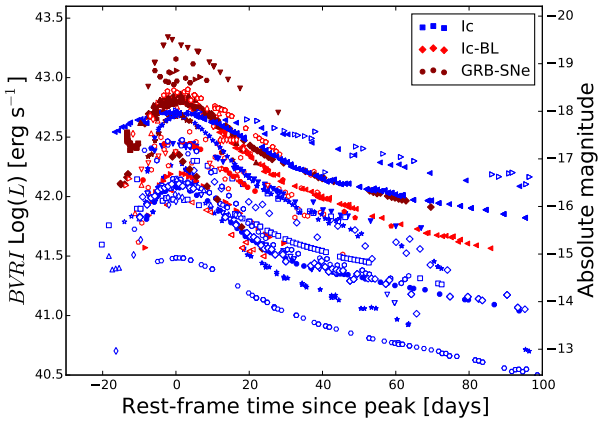

Figure 5. *BVRI* light curves of all Type Ic variants in the sample. SNe denoted by open markers have not been corrected for host-galaxy extinction. Markers may differ from the legend to aid the eye.

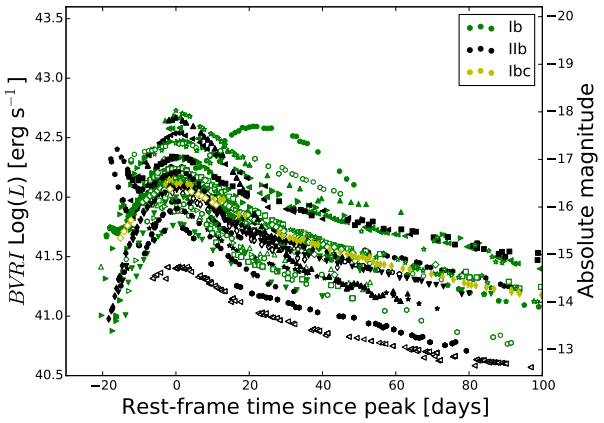

Figure 6. *BVRI* light curves of SNe Ib and SNe IIb in the sample. Open symbols represent SNe without a correction for host-galaxy extinction. Markers may differ from the legend to aid the eye.

Table 5. The *BVRI* luminosity-function statistics.

Type	Median	Mean	Standard deviation
SNe Ic-BL/GRB-SNe	42.81	42.78	0.29
SNe Ic	42.29	42.36	0.28
SNe Ib	42.33	42.34	0.27
SNe IIb	42.19	42.14	0.26

while this is somewhat driven by the GRB-SNe, it can be seen from Figure 5 that SNe Ic-BL are typically more luminous than other SNe Ic. The least-luminous subpopulation is SNe IIb. The standard deviation derived for each subset shows that there is considerable overlap between SNe Ic, SNe Ib, and SNe IIb.

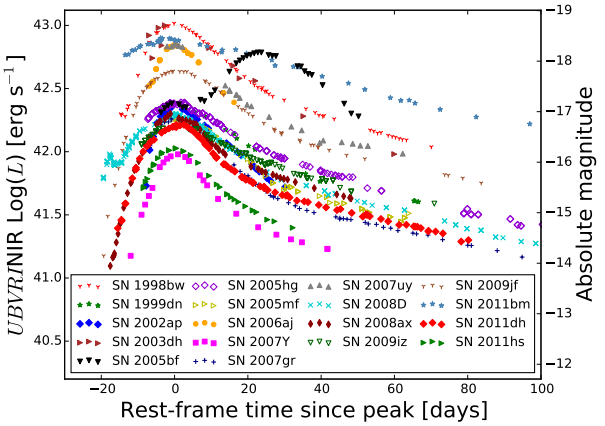

Figure 7. 18 *UBVRI*+ NIR pseudobolometric light curves constructed from optical and NIR photometry. Open symbols represent SNe without correction for host-galaxy extinction

5.3 Parameter values and statistics

With the bolometric light curves complete, we are now in a position to begin determining their properties. The following parameters are of interest:

- Peak luminosity — $L_{\rm p}$
- Rise time from explosion to $L_{\rm p}$ — $t_{\rm p}$
- Rise time from $L_{\rm p}/2$ to $L_{\rm p}$ — $t_{-1/2}$
- Decay time from $L_{\rm p}$ to $L_{\rm p}/2$ — $t_{+1/2}$
- Light-curve width — $t_{-1/2} + t_{+1/2}$
- Nickel mass — $M_{\rm Ni}$
- Ratio of ejecta mass to kinetic energy — $M_{\rm ej}^3/E_{\rm k}$

The statistics were found using the set of *BVRI* and *UBVRI*NIR-equivalent LCs. The first step was to determine the values of $L_{\rm p}$, $t_{-1/2}$, and $t_{+1/2}$. A fourth-order polynomial was fit to each light curve around the peak using CURVE_FIT from the PYTHON SCIPY[4] package. If the photometric coverage was sufficient, then the three parameters could be determined. However, in most cases only $L_{\rm p}$ plus one other of the temporal values was directly measurable. In the instances where the photometric observations did not extend sufficiently far before or after $L_{\rm p}$ to return $t_{-1/2}$ or $t_{+1/2}$, it may have been possible to extrapolate to this time if the initial/final luminosity was sufficiently close to $L_{\rm p}/2$. In an attempt to derive $t_{-1/2}$, a second-order polynomial was fit to the early-time observations up to the time of peak luminosity, provided a sufficient number of observations was available. If the fit could converge to a solution within two days of the boundary data point it was accepted. Conversely, on the rare occasion when $t_{+1/2}$ could not be taken directly from the observations, the late-time data were fit with a linear function and extrapolated out to five days to find a solution. The extrapolations were inspected visually for irregularities and accepted if they seemed reasonable. To derive estimates of the uncertainty, the upper and lower photometric errors were fitted in a similar fashion as previously described. In some cases, it was not possible to determine one or more

[4] www.scipy.org

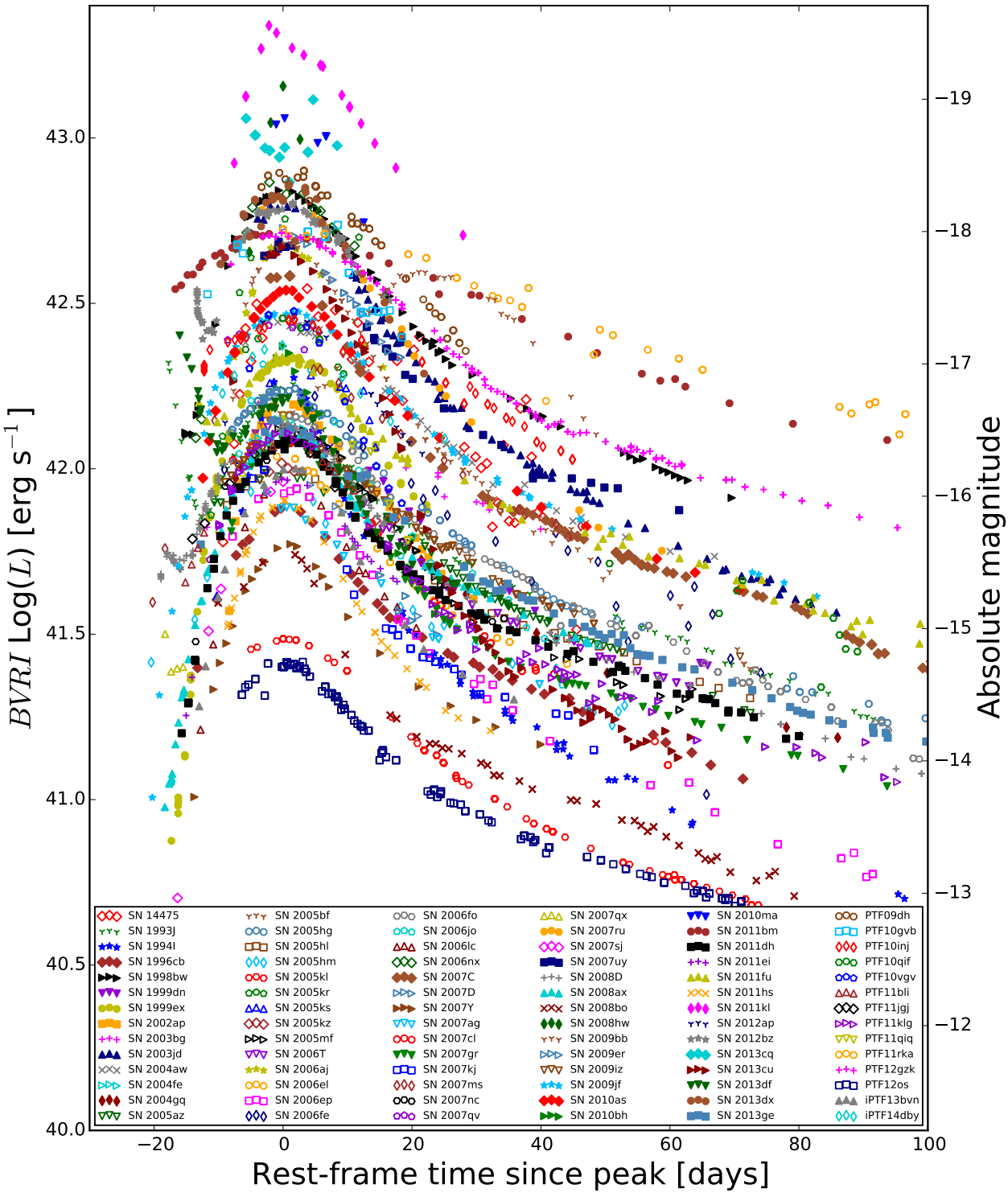

Figure 8. 84 *BVRI* light curves of all SN types in the sample. GRB-SN 2003dh is not included because it lacks a *BVRI* light curve. Note that GRB-SN 2013cq is extremely noisy, and its peak luminosity is constrained by a *Hubble Space Telescope* observation (Melandri et al. 2014). Open symbols represent SNe without corrections for host-galaxy reddening.

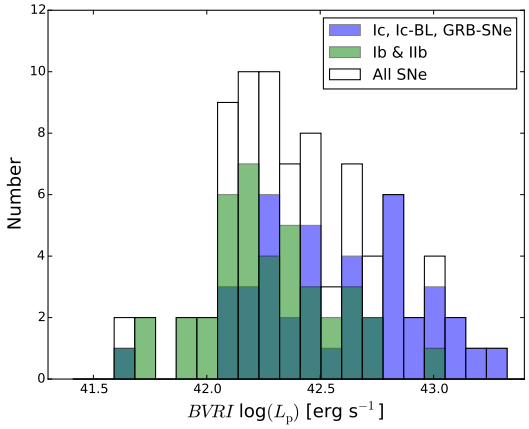

Figure 9. The *BVRI* pseudobolometric luminosity function of 82 SNe. The two SNe of Type Ibc are not included owing to ambiguity in their classification, nor is SN 2003dh owing to the lack of a *BVRI* LC. This distribution includes SNe with a correction for the median host-galaxy extinction of that type applied. The dark-green region represents the overlap of the blue and green distributions. The luminosity function for the combined green and blue distributions is shown in white.

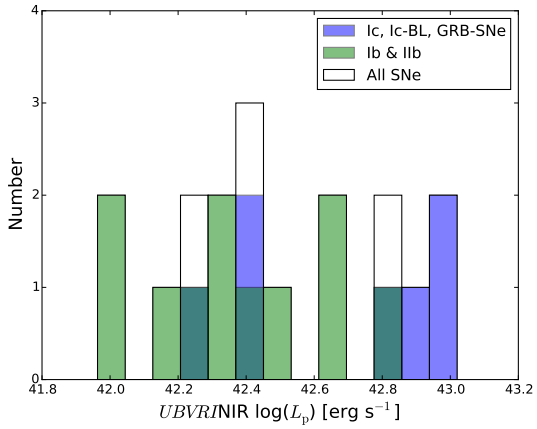

Figure 10. The luminosity function derived from the peak luminosity of the 18 *UBVRI*NIR light curves in the sample. Median host-galaxy extinction is assumed in three cases for statistical purposes. Colours are as described in Figure 9.

of these parameters, and so these SNe are omitted from the initial studies involving this parameter.

Table 6 gives the median temporal characteristics as derived from the *BVRI* group; we note that these values remain consistent with those derived for the *UBVRI*, *BVRI*NIR, and *UBVRI*NIR samples. We caution the reader that the median width is not the sum of the median values of $t_{-1/2}$ and $t_{+1/2}$ but is the median of the sum of the two parameters for SNe where both have been derived. This means that the median width is drawn from a smaller sample size than either $t_{-1/2}$ or $t_{+1/2}$. In particular the large median value of $t_{+1/2}$ for SNe Ic is largely driven by the extremely broad light curves of SNe 2011bm (Valenti et al. 2012) and PTF11rka, neither of which can be included in the calculation of median width

Table 6. Median temporal values derived from the *BVRI* data.

Type	$t_{-1/2}$ (days)	$t_{+1/2}$ (days)	Width (days)
SNe Ic-BL/GRB-SNe	$8.6\pm^{1.9}_{1.1}$	$15.1\pm^{1.0}_{2.0}$	$24.7\pm^{2.7}_{2.3}$
SNe Ic	$9.3\pm^{2.6}_{1.1}$	$19.2\pm^{4.7}_{5.4}$	$23.8\pm^{7.3}_{5.4}$
SNe Ib	$11.2\pm^{2.2}_{1.4}$	$17.0\pm^{2.8}_{2.9}$	$26.4\pm^{3.6}_{3.9}$
SNe IIb	$10.1\pm^{1.2}_{0.4}$	$15.3\pm^{2.8}_{1.6}$	$25.4\pm^{2.3}_{0.8}$

because they lack a value for $t_{-1/2}$. The relationship between $t_{-1/2}$ and $t_{+1/2}$ is considered in more detail in section 7.2.

In the Appendix, Table B1 and Table B2 give the values derived for individual SNe from the *BVRI* sample and the *UBVRI*NIR-equivalent sample, respectively.

5.4 Determining Errors

The error in any particular value derived is related to the uncertainties in the photometry and the extinction. In certain situations the photometric errors are very small, perhaps unjustly so, which is the cause of very small uncertainties in the values determined in this section. Very small uncertainties lead to a higher degree of certainty in a value than is justified, and they have the effect of biasing possible correlations between parameters by increasing the weighting of the values for a particular SN. Ideally, a well-observed SN with good Galactic and host-galaxy extinction would have such an effect, but we see that some SNe which fall short of this standard display extremely small uncertainties in their photometry. It can be seen in the LCs of these SNe that the uncertainties are unjustified, as they show variability which is greater than the photometric errors bars.

5.5 Rise time

The parameter with the largest uncertainty is rise time, t_p, principally because it requires well-covered photometry pre-peak and because of the uncertain behaviour of the light curve at very early times. Generally, only GRB/XRF SNe have an observed value of t_0 and hence a well-constrained t_p, although the explosion time of SNe IIb with prominent early-time emission (e.g., SN 1993J, Matheson et al. 2000; SN 2013df, Van Dyk et al. 2014; SN 2011dh, Arcavi et al. 2011; SN 2013cu, Gal-Yam et al. 2014) caused by the cooling of the stellar surface following shock breakout (Woosley et al. 1994) can be estimated to within a day or two of explosion. If the SN is found in a host galaxy that is regularly observed, then t_0 can be constrained between the detection and nondetection dates assuming that $\langle dL/dt \rangle$ is sufficiently large at early epochs so as to minimise the "dark time" (the period between explosion and detectability) of the SN (e.g., PTF10vgv; Corsi et al. 2012). Of course, this method is limited to the time interval between the two dates, which ideally should be on the order of a few days. Values for t_p from the literature are given in Table 7.

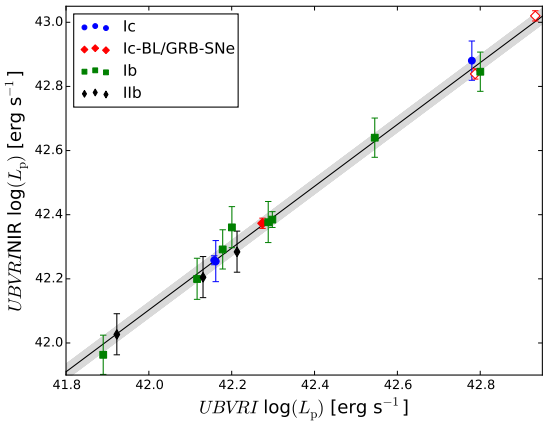

Figure 11. *UBVRI*+NIR peak luminosity as a function of *UBVRI* peak luminosity. The correlation appears to be independent of SN type. The grey area represents the 1σ uncertainty in the fit determined by the standard deviation of the residuals. The error bars are representative of the uncertainty only in the NIR contribution. Open symbols represent GRB-SNe.

5.6 Comparison between optical and optical/NIR light curves at peak

We took the step of plotting the *UBVRI* luminosity at maximum versus *UBVRI*NIR maximum luminosity to investigate the possibility of determining some form of "bolometric correction" for the much larger *BVRI*-only sample. The results of this test are shown in Figure 11. It is apparent, at a glance, that all SNe in this set follow a very tight correlation between the two values, and while caution must be exercised when dealing with values in log-log space, it appears that a simple linear fit would produce the desired results. The data were fit with a simple linear polynomial of the form given by the equation

$$\log(L_{UBVRINIR}) = a_1 + a_2 \log(L_{UBVRI}) \quad (1)$$

The best fit gives $a_1 = 1.62$ and $a_2 = 0.96$ with the standard deviation of the residual distribution equal to 0.02, which is adopted as the uncertainty in the fit. The SN with maximum displacement from the best-fit line shows a difference of $<$ 20% between the value returned from the polynomial and the photometric value.

Overall, it appears that the variation in spectral shape is less important outside the optical wavelengths. This correlation is also very strong for *BVRI* against *BVRI*NIR. Thus, the conversion to fully bolometric luminosity requires little more than a simple multiplicative factor that is proportional to the optical flux. This implies that, around peak luminosity, the absorption and re-emission of photons as they diffuse through the ejecta happens primarily in the optical regime. Consequently, the NIR region is effectively the Rayleigh-Jeans tail of a blackbody with a temperature that gives an optical integrated flux similar that of the SN optical SED.

6 PSEUDOBOLOMETRIC TO FULLY BOLOMETRIC

The disparity in number of SNe with *BVRI* data compared with *UBVRI*NIR data presents a challenge to efforts to reveal the statistics of the explosion, especially the luminosity function and the mass of ^{56}Ni synthesised in the first seconds after core collapse. Here we detail how we construct fully bolometric peak luminosity values for all the SNe in the sample using the results from earlier sections.

6.1 The conversion method

To minimise the amount of uncertainty in each SN, the shortest method of obtaining the fully bolometric peak luminosity was used. The details of this procedure are outlined here.

6.1.1 Conversion from BVRI to UBVRI at peak

Approximately half of the SNe in the database lack U/u' photometry. To compensate for this, we use the results of Section 3.7 and apply a correction to account for the missing photometric band to the *BVRI* flux of these SNe. We use Table 4 to assign a correction value depending on SN type and whether there is a value for host-galaxy extinction. We assume the errors are commensurate with the standard deviation of each distribution. As a justification, we note that from Table 4 the median U fraction is always between 15% and 20%.

6.1.2 Conversion from UBVRI to UBVRINIR

There are two pathways to convert the *UBVRI* flux to *UBVRI*NIR flux. In the first instance we can use the NIR data where they exist and combine their peak value with that of the *UBVRI* flux. The second method utilises Equation 1 and the values for the *UBVRI* to *UBVRI*NIR conversion as given in Section 5.6.

6.1.3 UBVRINIR to fully bolometric

We finalise the conversion of *UBVRI*NIR L_p to a fully bolometric value by assuming a 10% contribution from unobserved wavelengths. We justify this value by integrating a Planck function at temperatures between 4000 K and 8000 K, which is typical for SE-SNe at peak, and comparing the flux ratio of our *UBVRI*NIR wavelength range to that of the flux outside it. We find that the UV and far-infrared can account for between $\sim$ 7% and $\sim$ 20% of the total flux but is typically $\sim$ 10%. If we assume some reprocessing of UV photons into the optical regime then this value can be lower. Thus, we take the error to be +10%–5%. We do not attribute any particular fraction of this amount to IR or UV, the latter of which is small for SE-SNe (Pritchard et al. 2014).

6.2 Luminosity function for the bolometric sample

The resulting fully bolometric luminosity function for the entire SN sample is shown in Figure 12 and the statistics

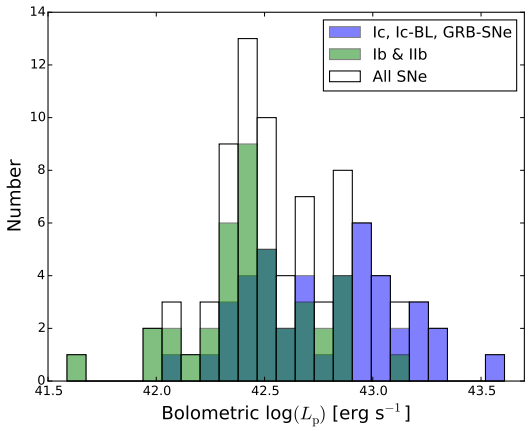

Figure 12. Fully bolometric luminosity function of the entire sample. Median host-galaxy extinction is adopted when the actual value is absent. Colours are as described in Figure 9.

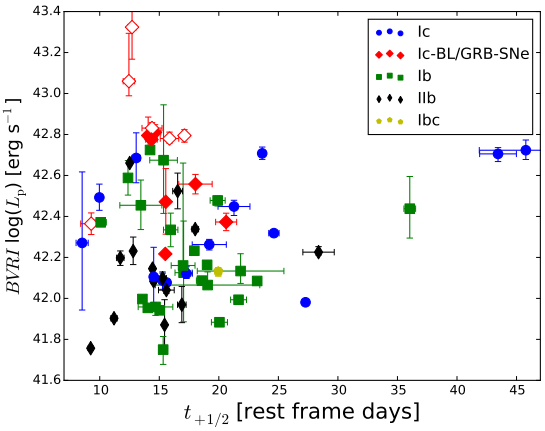

Figure 13. L_p as a function of $t_{+1/2}$ for the $BVRI$-equivalent light curves. There is no correlation between either parameter. Open symbols represent GRB-SNe.

are shown in Table 10. The SN Ic/Ic-BL/GRB-SN group remains the most luminous population. SNe Ic and SNe Ic-BL can be found throughout this distribution while GRB-SNe occupy the upper end.

7 TEMPORAL PROPERTIES

7.1 L_p as a function of $t_{+1/2}$

The value of Type Ia SNe for cosmological studies owing to the correlation between B-band peak and light-curve decline over 15 days (Phillips 1993) is well known. All previous attempts to find a similar relation for core-collapse SNe have returned negative results (Drout et al. 2011; Lyman et al. 2014). Figure 13 shows how the $BVRI$ pseudobolometric peak of our sample compares with $t_{+1/2}$. It is apparent that there is no equivalent "Phillips relation" for any SN type used here, thus confirming earlier studies and indicating that the dynamics of the explosion mechanism of SE-SNe and the relationship to the ejecta is nonuniform.

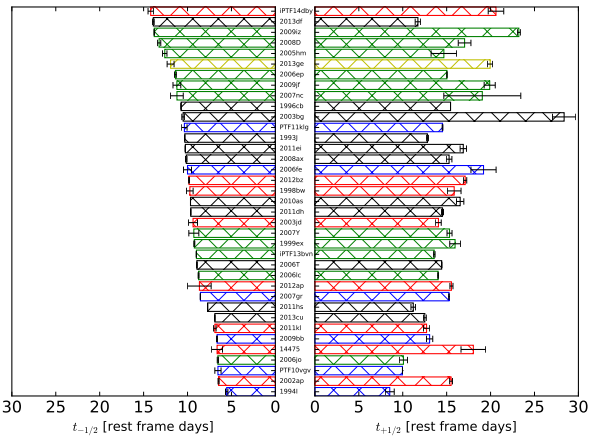

Figure 14. The $t_{-1/2}$ and $t_{+1/2}$ values for the SNe in the sample with both parameters. The range of values in $t_{+1/2}$ is readily apparent despite a trend of the decay time to increase as the rise time increases. SNe Ib are shown in green, Ic-BL/GRB-SNe are red, Ic are blue, IIb are black, and Ibc are yellow.

7.2 Is there a relationship between $t_{-1/2}$ and $t_{+1/2}$?

Photometric coverage in not consistent across the whole sample, so a full set of temporal parameters is available only for a small number of SNe. Motivated by the desire to maximise the statistics derived from our sample, we examined temporal parameter values as a function of other temporal characteristics where the values were known. A plot of $t_{-1/2}$ and $t_{+1/2}$ indicated that a loose correlation exists. We removed SNe that showed an excess of luminosity caused by shock breakout and nonradioactive power, further strengthening the apparent correlation between the two properties. However, this is at odds with the results of Taddia et al. (2015), where the Kolmogorov-Smirnov (K-S) tests on the value of Δm_{15} for the r band for 40 SNe indicated that they were drawn from the same population.

Consequently, we performed a similar analysis on our $t_{+1/2}$ values. Figure 14 shows $t_{+1/2}$ as a function of $t_{-1/2}$. It can be seen that although there is a general trend to a slower decline for a slower rise, there is a considerable spread in the values. We plotted cumulative distribution functions (CDFs) for all $t_{+1/2}$ values derived in the sample and split them by type, as seen in Figure 15. K-S tests indicate that most of the distributions are drawn from the same population ($P > 0.05$) with the exception of the SN Ic/IIb group ($P = 0.048$), although the SN Ic/Ic-BL group returns $P = 0.061$ which is marginally over the threshold. We can attribute this entirely to the presence of broad light curve SNe Ic 2011bm and PTF11rka in conjunction with the relatively small number of SNe throughout: 12, 14, 23, and 13 for SNe Ic-BL, Ic, Ib, and IIb, respectively. It is clear that these two SNe disproportionately affect the sample, because without their presence the SN distributions are very similar, sharing a similar median $t_{+1/2}$ of $\sim$ 15 days. With this result, we cannot conclude that there is a significant correlation between $t_{-1/2}$ and $t_{+1/2}$, and while the general trend is toward a longer decay for a longer rise, the variance along the trend makes it unreliable as a method for converting one to the other.

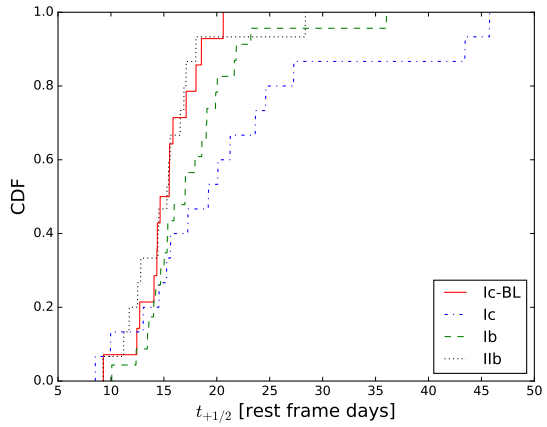

Figure 15. The cumulative distribution function of all the $t_{+1/2}$ values in the sample sorted by spectral type. The effect of the extremely slowly declining Type Ic SNe 2011bm and PTF11rka on the SN Ic CDF is clearly seen.

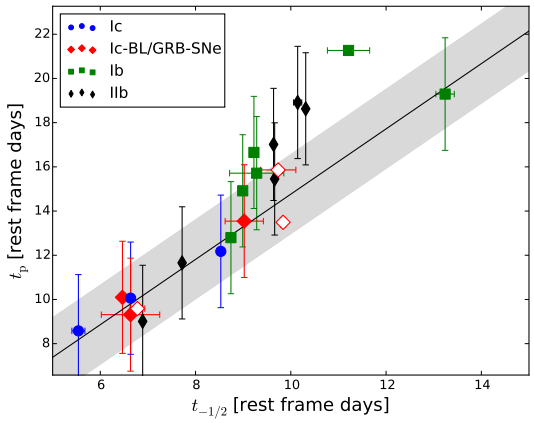

Figure 16. t_p as a function of $t_{-1/2}$ for SNe in the sample having both parameters. The black line represents the best fit to the data incorporating errors in both the ordinate and abscissa. The grey region represents the standard deviation of the residuals from this line, which is taken to be the uncertainty in the fit. Open symbols represent GRB-SNe.

7.3 Correlation between t_p and $t_{-1/2}$

It is pertinent to see if the time for rise to peak of the SN is in some way correlated with the rise from $L_p/2$ to L_p, as it would lead to a method to estimate the SN rise time from $t_{-1/2}$. The limitations of such an assessment are apparent, as few SNe have known explosion times. Thus, we take the GRB-SNe with their known t_0, some of the SN IIb set (because their explosion times can be constrained from the initial shock-breakout peak), plus any SN with well-constrained explosion time owing to the short interval between nondetection and detection. Figure 16 shows t_p against $t_{-1/2}$; it is apparent that there is some correlation which appears to be independent of SN type. Using a linear fit as before, defined as

$$t_p = \alpha t_{-1/2}, \tag{2}$$

we find $\alpha = 1.5$. To determine uncertainties in the fit we took the standard deviation of the distribution of the residuals as described previously, which we find to be 1.68 days. SNe were omitted from the fitting procedure if the early-time emission was dominated by shock breakout. These were typically SNe IIb or GRB-SNe for which $t_{-1/2}$ was poorly constrained owing to two components, and well-defined explosion times heavily influenced the result.

7.4 Inferred rise time t_p

Table 7 shows the inferred rise time for the sample as derived by the previously described correlation. Note that the rise times for GRB-SN 1998bw ($\sim$ 16 days) and GRB-SN 2006aj ($\sim$ 10 days) are recovered within the uncertainties of the extrapolated explosion time. Notable exceptions are as follows. (i) SNe that show relatively slowly declining shock break-out emission so that it is a nonnegligible contributor to the flux of the SN during the rise (e.g., SN 2008D, SN 2011hs). (ii) The case of SN 2011kl, associated with ultralong GRB 111209A (Greiner et al. 2015); this SN is interesting with regard to the explosion mechanism.

First, we must consider an explanation for the correlation between $t_{-1/2}$ and t_p. This can be explained by the interplay with ^{56}Ni $\rightarrow$ ^{56}Co $\rightarrow$ ^{56}Fe energy injection and the light-curve rise time, which is itself a function of opacity, ejecta mass, and photospheric velocity (Arnett 1982). Because the derivative of the energy injection rate is constant, the shape of the light curve is determined solely by the diffusion time. Altering the diffusion time means the peak may move, but the way the light curve rises to the peak retains the same relative shape provided the nickel distribution remains located centrally. This is not necessarily the case for an alternate energy source such as a magnetar, where the magnetar rotational energy can be deposited into the ejecta on a timescale much less, or much greater, than the diffusion time, or the case where shock breakout (particularly for SNe IIb) or GRB afterglow contribute to the optical flux. For all GRB-SNe, except SN 1998bw where the GRB afterglow was negligible, afterglow subtraction is a major issue for accurately determining $t_{-1/2}$; fortunately, the need for this value is made redundant by a known explosion date.

8 EXPLOSION PROPERTIES

8.1 The synthesis of ^{56}Ni

With the fully bolometric L_{peak} and t_p, it is now possible to estimate the amount of ^{56}Ni synthesised in the explosion. To obtain a value for M_{Ni}, we used the formulation from Stritzinger & Leibundgut (2005) which is based upon "Arnett's rule" (Arnett 1982): the approximation that the maximum luminosity of a SN powered by the decay of ^{56}Ni is equal to the energy released by radioactive decay at that time:

$$\begin{aligned}\frac{M_{Ni}}{M_\odot} =& L_p \times \left(10^{43}\mathrm{erg\ s^{-1}}\right)^{-1} \\ &\times \left(6.45 \times e^{-t_p/8.8} + 1.45 \times e^{-t_p/111.3}\right)^{-1}\end{aligned} \tag{3}$$

Table 7. $t_{\rm p}$ values.

SN	Literature $t_{\rm p}$	$t_{\rm p}$ from $t_{-1/2}$
1993J	19.15±0.03	16.32±1.65
1994I	12.25±0.21	8.77±1.66
1996cb	-	16.99±1.65
1998bw	15.86±0.18	15.41±1.69
1999dn	13.92±2.84	-
1999ex	18.35±0.04	14.60±1.65
2002ap	13.01±0.00	10.23±1.65
2003bg	-	16.62±1.66
2003dh	12.65±1.66	-
2003jd	12.50±0.18	14.83±1.73
2004fe	-	14.68±1.65
2005bf	18.32±0.35	-
2005hm	-	19.93±1.67
2005kr	-	11.41±1.67
2005ks	-	12.37±1.66
2006T	-	14.15±1.65
2006aj	9.59±0.04	10.73±1.66
2006ep	-	18.00±1.65
2006fe	-	15.83±1.71
2006jo	-	10.37±1.65
14475	-	10.50±1.76
2006lc	-	13.84±1.65
2006nx	-	14.28±1.70
2007Y	18.76±0.35	14.69±1.75
2007gr	13.15±0.23	13.50±1.65
2007ms	-	22.23±1.67
2007nc	-	17.73±1.80
2007qx	-	15.09±2.76
2007ru	10.24±0.05	-
2007sj	-	14.54±1.66
2007uy	19.08±0.28	-
2008D	19.29±0.23	20.95±1.66
2008ax	19.28±0.13	16.05±1.65
2008hw	12.31±0.10	-
2009bb	12.63±0.10	10.50±1.65
2009iz	-	21.83±1.65
2009jf	21.27±0.16	17.74±1.71
2010as	12.44±0.12	15.29±1.65
2010bh	12.74±0.10	5.20±1.68
2010ma	10.33±4.34	-
2011bm	34.59±0.15	-
2011dh	15.71±0.02	15.25±1.65
2011ei	17.73±0.03	16.22±1.65
2011hs	8.59±0.06	12.21±1.65
2011kl	15.17±0.07	10.90±1.66
2012ap	13.19±0.31	13.69±2.12
2012bz	13.49±0.22	15.57±1.65
2013cq	13.00±2.00	-
2013cu	9.01±0.08	10.90±1.65
2013df	21.79±0.10	21.99±1.65
2013dx	12.26±5.48	-
2013ge	-	18.88±1.70
PTF10vgv	-	10.35±1.69
PTF11bli	-	20.63±1.66
PTF11jgj	-	22.07±2.17
PTF11klg	-	16.39±1.68
PTF12gzk	16.35±0.46	-
iPTF13bvn	15.95±0.10	14.23±1.65
iPTF14dby	-	22.46±1.68

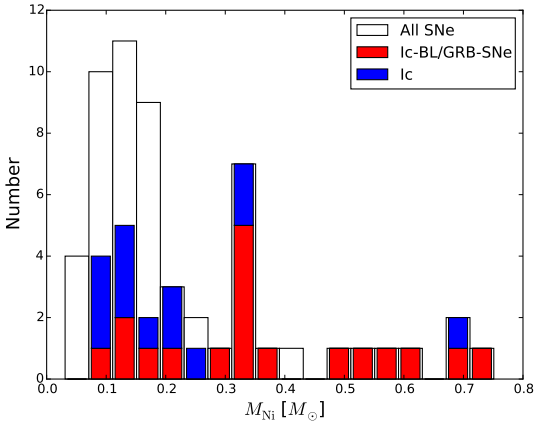

Figure 17. The ^{56}Ni distribution for the fully bolometric sample with the normal SNe Ic and the SNe Ic-BL/GRB-SNe in blue and red, respectively. Consistent with our procedure for the bulk analysis, corrections for median host-galaxy extinction have been applied. The bulk nickel-mass distribution, for SNe where the nickel mass can be derived, is shown in white.

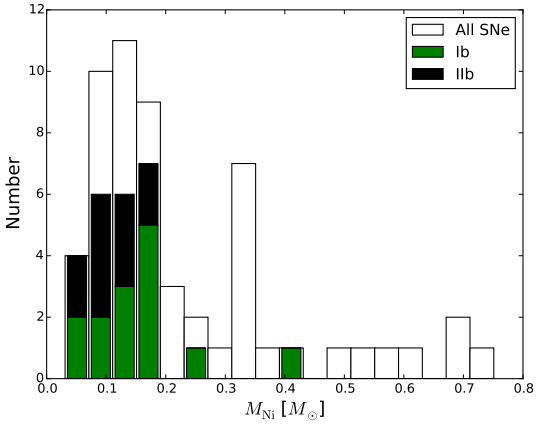

Figure 18. The ^{56}Ni distribution for the fully bolometric sample with the normal SNe Ib and SNe IIb in green and black, respectively. Corrections for median host-galaxy extinction have been applied. The white region is the same as in Figure 17.

We use equation 3 to evaluate $M_{\rm Ni}$ for the *BVRI*, *UBVRI*NIR, and the fully bolometric sample. We adopt the exact value of $t_{\rm p}$ if known; failing that, we adopt the $t_{-1/2}$ to $t_{\rm p}$ conversion (Equation 2) to reduce the propagation of uncertainties. The result of this is given in Table B3. The $M_{\rm Ni}$ distribution for the whole sample, highlighting SNe Ic/Ic-BL and GRB-SNe, is shown in Figure 17, whereas Figure 18 the whole sample emphasises SNe Ib and SNe IIb. The spread of synthesised $M_{\rm Ni}$ varies between SN types. The SN Ic group shows the largest spread while the SN Ib and SN IIb populations cluster toward the lower end of the distribution. The normal (i.e., non-broad-lined) SNe Ic also include the non-GRB-SN with the largest nickel mass, SN 2011bm, which is a consequence of its exceptionally broad light curve. Figure 19 gives peak bolometric luminosity as a function of $M_{\rm Ni}$ for the sample.

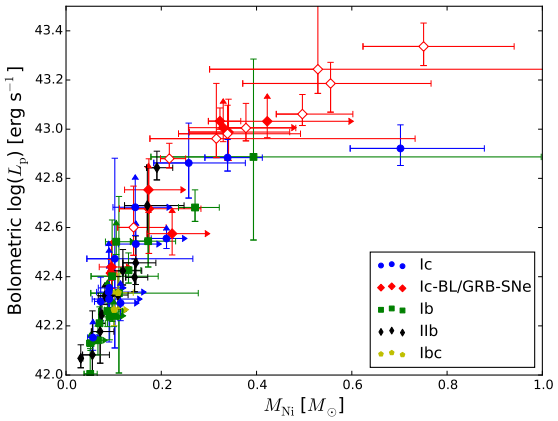

Figure 19. Peak bolometric luminosity as a function of nickel mass. Open symbols represent GRB-SNe.

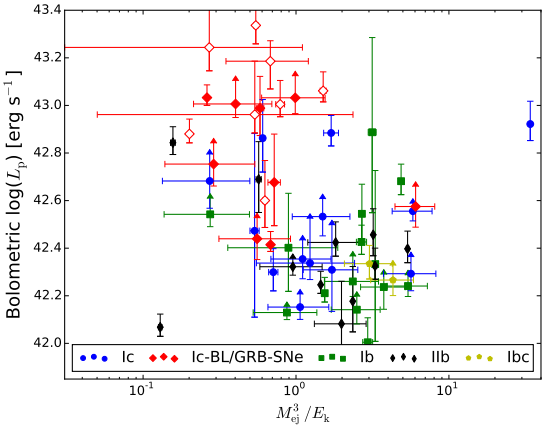

Figure 20. Peak bolometric luminosity as a function of $M_{\rm ej}^3/E_{\rm k}$. Open symbols represent GRB-SNe.

8.2 Characteristic timescales, kinetic energy, and ejecta mass

The rise time of the SN is linked to the powering mechanism, the spatial distribution of ^{56}Ni, the opacity of the ejecta (κ), the mass of the ejecta ($M_{\rm ej}$), and the photospheric velocity at luminosity peak $v_{\rm ph}$ via the formulation for the parameter τ_m given by Arnett (1982),

$$\tau_m = \sqrt{2}\left(\frac{k}{\beta c}\right)^{\frac{1}{2}}\left(\frac{M_{\rm ej}}{v_{\rm ph}}\right)^{\frac{1}{2}}. \quad (4)$$

For ejecta of uniform density undergoing spherically symmetric free expansion ($R(x,t) = v(x)t$), we can convert $v_{\rm ph}$ to $E_{\rm k}$ via Equation 5,

$$E_{\rm k} = \frac{3}{10}M_{\rm ej}v_{\rm ph}^2, \quad (5)$$

which leads to

$$\tau_m = \left(\frac{\kappa}{\beta c}\right)^{\frac{1}{2}}\left(\frac{6M_{\rm ej}^3}{5E_{\rm k}}\right)^{\frac{1}{4}}, \quad (6)$$

where β is a constant of integration with value of ~ 13.7. The parameter τ_m, which defines the scale time of the light curve, is similar to the rise time of the SN but typically lower by ~ 2 days. However, by assuming that $t_{\rm p} \approx \tau_m$, we can estimate a value for $M_{\rm ej}^3/E_{\rm k}$ for a range of opacities; see Table B4. Note that this model assumes that κ is independent of time and constant across the ejecta — but this is not true for any SN, especially SNe Ib and SNe IIb. In these cases the opacity of the He shell is extremely low owing to the paucity of He lines in the optical. Consequently, the value for $M_{\rm ej}$ derived from τ_m underestimates the total mass of the ejecta because the photons emitted from the photosphere diffuse through this shell with little overall interaction (also see Wheeler et al. 2015).

We plot $L_{\rm p}$ and $M_{\rm Ni}$ as a function of $M_{\rm ej}^3/E_{\rm k}$ in Figures 20 and 21. There is considerable scatter in each plot, but for a given value of $L_{\rm p}$ or $M_{\rm Ni}$ the value of $M_{\rm ej}^3/E_{\rm k}$ tends to be higher for SNe Ib and SNe IIb compared with SNe Ic. The width of SN 2011bm leads to a large value for $M_{\rm ej}^3/E_{\rm k}$, which in turn necessitated the use of a logarithmic abscissa.

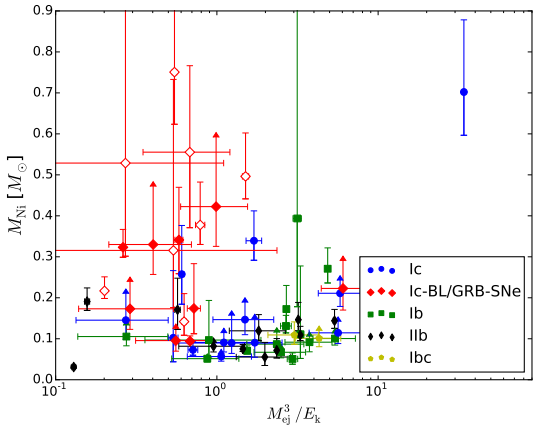

Figure 21. Nickel mass as a function of $M_{\rm ej}^3/E_{\rm k}$. Open symbols represent GRB-SNe.

9 COMPARISON WITH MULTIBAND PHOTOMETRY

9.1 Deriving multiband parameters

The multiband photometry of each SN was fit using the same process as described in Section 5.3. The raw photometry was dereddened for Galactic extinction in the observer frame and host-galaxy extinction in the rest frame, where possible.

9.2 Colour curves

The diversity of filters used in the observations implies that there is no single colour that can be used to represent every SN in the sample as is; this requires the use of some filter conversion to homogenise the sample. We utilise the colour corrections of Jordi et al. (2006) to convert B and V to g' and R to r', so as to present the $g'-r'$ colour for all of the SNe. This is the most sensible choice for conversion because g' lies between B and V while r' lies blueward of R, so the conversions fall between the available photometry. We note that this process is not perfect and stellar colour transformations can be poor for emission-line objects. How-

ever, it should be less of an issue during the photospheric phase ($\lesssim$ 40 days) when the spectrum can be more closely approximated by a blackbody.

As a test of the accuracy of this conversion we utilise SN PTF12gzk, which has photometry in *UBVRIgriz*. We find that the transformed colour falls within the uncertainties of that determined directly from the photometry, giving confidence that this method is sufficiently accurate within the bounds of the photometric uncertainties.

We take the approach of plotting the colours of all SNe at $z < 0.05$ with extinction corrections applied only when the reddening is known. The limit on distance is chosen so as to minimise the need for K-corrections, which become more important at $z > 0.05$. This importance is amplified by the behaviour of g' and r', as they lie on opposite sides of the SED peak for most SNe until times much later than the peak of the bolometric LC. The behaviour of the K-correction is dependent on the underlying spectrum, the epoch, and the redshift, which can have a dramatic effect on the colours as g' and r' can be corrected in opposite directions. For example, at $\sim$ 10 days past bolometric maximum and in the $z < 0.05$ regime, the K-correction in the g' band is typically $\sim$ 0 mag, but it begins to rise rapidly to $\sim$ 0.1 mag as z tends to 0.05. In the r' band the behaviour is more complex, with the low-z K-correction taking small positive or negative values but tending toward lower values as z increases. At other times the behaviour can be different and more extreme, especially with increasing redshift. Hence, we limit this effect by restricting the sample to low z.

Figure 22 shows the $g' - r'$ colour evolution over the photospheric phase; SNe without known host-galaxy extinction are plotted in transparent markers to separate them. When host extinction is applied the spread of colours narrows, and at $\sim$ 10 days past bolometric peak it forms a "bottleneck"; see Figure 23. This behaviour is similar to that seen by Drout et al. (2011) in the $V - R$ colours of their sample, and was similarly observed for SNe with $g - r$ by Taddia et al. (2015). The colour evolution of SN 2005bf is unique and appears to reflect the light curve, with the blue dips being approximately coincident with the luminosity peaks. If one was to take the second peak as the bolometric maximum, then the colour curve would shift to the left by 20 days and line up with the other SNe. Type IIb SN 2011hs, $E_{\rm host}(B - V) = 0.16 \pm 0.07$ mag (Bufano et al. 2014), is a notable outlier in Figure 23. Bufano et al. (2014) find that $g' - r'$ is $\sim$ 0.6 mag around the time of g' maximum and there is a $\sim$ 0.5 mag difference between the colours of SN 2011hs and SN 2008ax. The result here is comparable, with $g' - r' \approx 0.6$ mag in the few days before bolometric maximum and a similar difference between the two SNe, which is consistent with the period around g' maximum. It may be that the host extinction has been underestimated in this case, or it could be indicating that not all SNe sit within the main distribution.

Figures 24 and 25 show the colour evolution of SNe split by spectral type for all SNe Ic and SNe Ib/IIb, respectively. The "bottleneck" is more readily apparent in the SN Ic/Ic-BL/GRB-SN population than it is for SNe Ib/IIb, providing further caution in attempting to use colours as a basis of determining host extinction. Note that for clarity, uncertainties are not shown in these figures.

Table 8. Effective wavelength when photometry peak matches bolometric peak.

SN Type	Median λ (Å)	$\langle\lambda\rangle$ (Å)	σ (Å)
Ic-BL	5449	5369	536
GRB-SNe	4869	5065	419
Ic	5616	5452	826
Ib	5416	5454	500
IIb	5308	5277	334

9.3 Comparing the multiband and bolometric peak time

The time of peak of the photometry is a function of the effective wavelength of the band, with blue bands peaking earlier than red bands (Taddia et al. 2015). This can be explained by the evolution of the underlying spectrum and the cooling of the photosphere, although absorption features can affect the temporal evolution of the photometry. By using the photometry and interpolating the time of peak between the bands we can estimate the wavelength peak that coincides with $t_{\rm p}$. Table 8 gives the average wavelength where the photometry would peak at $t_{\rm p}$; it can be seen that the values are around that of the V band, $\lambda_{\rm eff} = 5505$ Å. For GRB-SNe the SED can be "contaminated" by afterglow flux, which is preferentially blue, leading to a bluer SED peak. Unfortunately, it is hard to account for GRB afterglow beyond simple empirical methods (see Section 3.2). For comparison, the spectra of GRB-SN 1998bw are red, broad-lined, and almost featureless owing to the comprehensive reprocessing of optical photons to lower frequencies by the high-energy ejecta. SN 1998bw is significant in this regard because its SED peak is redder than the median for GRB-SNe ($\sim$ 5200 Å) and the afterglow was negligible, so the photometry and spectrum are not contaminated in the way that (for example) GRB-SN 2013dx is.

9.4 Bolometric corrections

In the era of large-scale surveys [e.g., PTF, iPTF, the Panoramic Survey Telescope and Rapid Response System (Pan-STARRS); the future Large Synoptic Survey Telescope (LSST) and the Zwicky Transient Facility (ZTF)], where the number of transients discovered has increased (and will continue to increase) by orders of magnitude, it is apparent that with a limited number of telescopes available, long-term multiband follow-up observations of single objects become more time consuming. Bolometric corrections are a useful way of approximating the bolometric luminosity from a single band or colour (Lyman et al. 2014), which in turn enables the determinations of the bolometric properties of the SN. To this end, we investigate the bolometric corrections (BCs) in single bands for our database.

The BC is defined as

$$M_{\rm band} - {\rm BC} = M_{\rm bol}. \quad (7)$$

To estimate the BC, we subtract $M_{\rm bol}$ at the time of bolometric peak from $M_{\rm band}$ at the time of peak in that band and calculate a distribution. The mean and standard deviation of each distribution is given in Table 9; the standard deviation

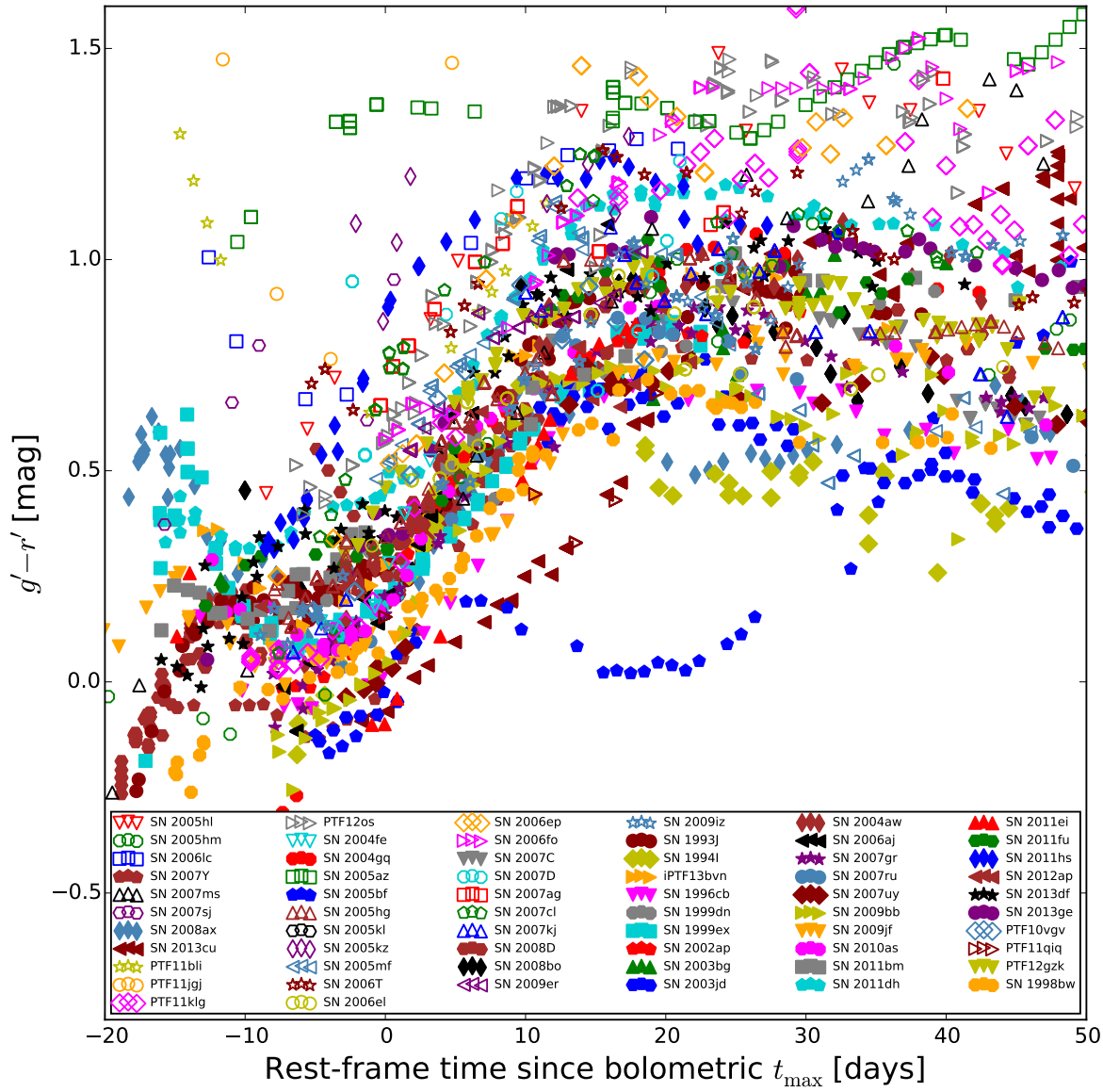

Figure 22. $g'-r'$ colour of the SNe in the sample at $z < 0.05$. Open markers indicate SNe where $E(B-V)_{\rm host}$ is not known. To see how correcting the colour curves for host extinction affects the spread, see Figure 23.

is taken to be the error of the bolometric correction δBC. It is apparent that the band with the least scatter is R, where $\delta BC = 0.13$ mag, followed by I ($\delta BC = 0.18$ mag); r' and i' are less constrained, with $\delta BC = 0.28$ mag and 0.27 mag (respectively). This is an issue for calculating BCs via this method because it relies on the spectral differences of each SN being outside the band in question. If R ($\lambda_{\rm eff} = 6580$ Å) and I ($\lambda_{\rm eff} = 8060$ Å) define such a region, then it should be expected that i' ($\lambda_{\rm eff} = 7630$ Å) would also be a tracer for the bolometric luminosity, but the scatter is actually considerably greater for this band. The reason behind this could possibly be systematics (e.g., relatively poor photometry), but this would have to be applicable to a large number of observations across many years to avoid being lost in the noise of better observations.

There is insufficient evidence to suggest that any particular band is a superior tracer of the bolometric light curve at peak. Additionally, if one were to apply the BC to some SNe, the returned luminosity would be poorly constrained. This is because the standard deviation of the spread of residuals

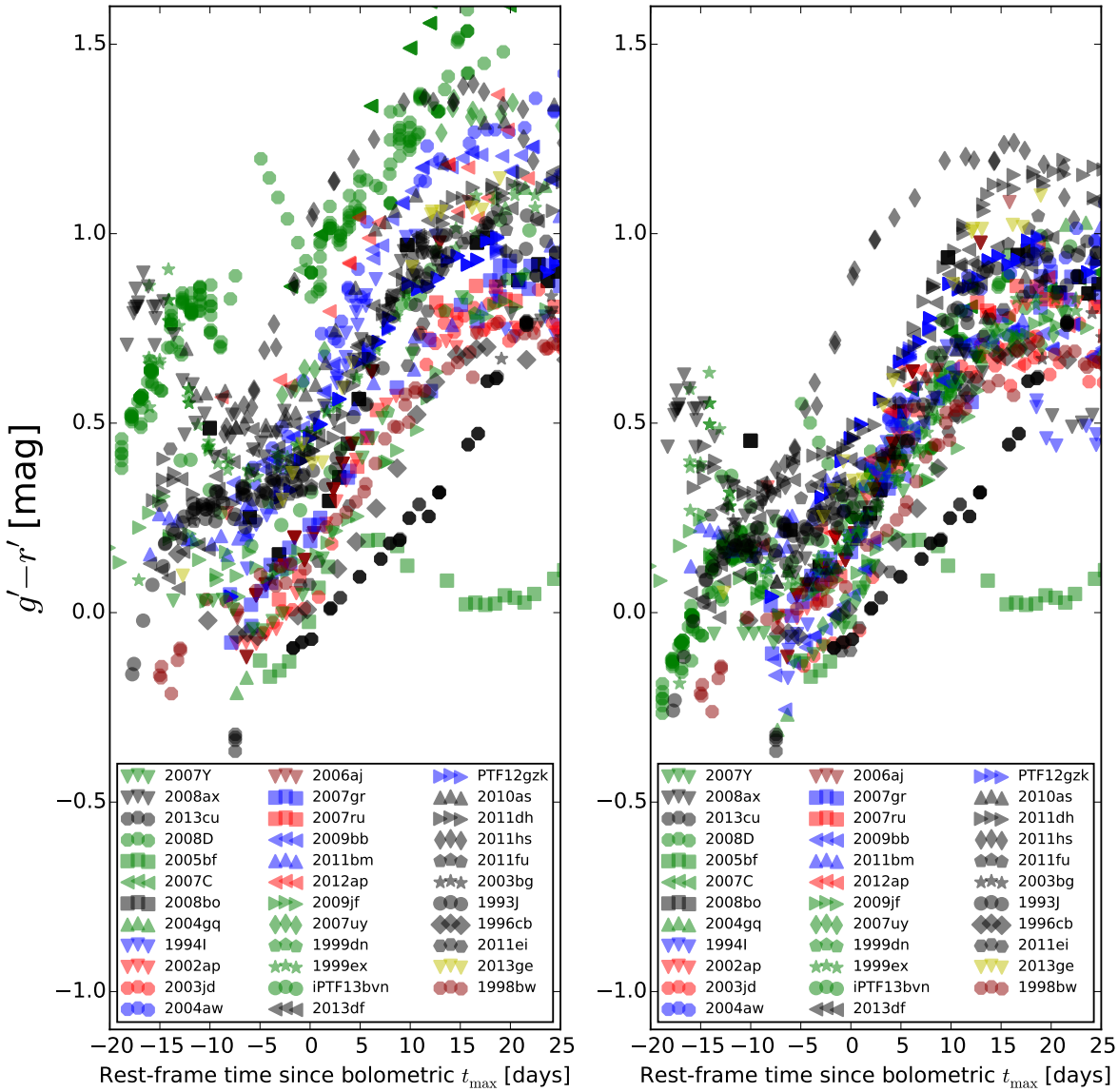

Figure 23. $g' - r'$ colour curves of the SNe in the sample at $z < 0.05$, sorted by spectral type, showing before (left) and after (right) correction for host extinction. SNe of Types Ic, Ic-BL, Ib, IIb, Ibc, and GRB-SNe are shown in blue, red, green, black, yellow, and dark red, respectively.

from the BC, which is taken to be the uncertainty in the resulting luminosity, corresponds to approximately a quarter of the value returned. Here we have yet to even consider errors in the input photometry. Given that the spread of SN luminosities typically ranges between 10^{42} erg s^{-1} and 10^{43} erg s^{-1}, this uncertainty represents a significant fraction of the parameter space; hence, the BCs are not applied here.

10 DISCUSSION

10.1 Biases

It would be remiss to fail to appreciate the biases involved in the data used for this study. SNe were rare discoveries until the early/mid 1990s. Typically fewer than 20 per year were discovered, but as technology improved and more large-scale surveys were initiated, the number count increased from a few tens per year to the few hundred discovered each year

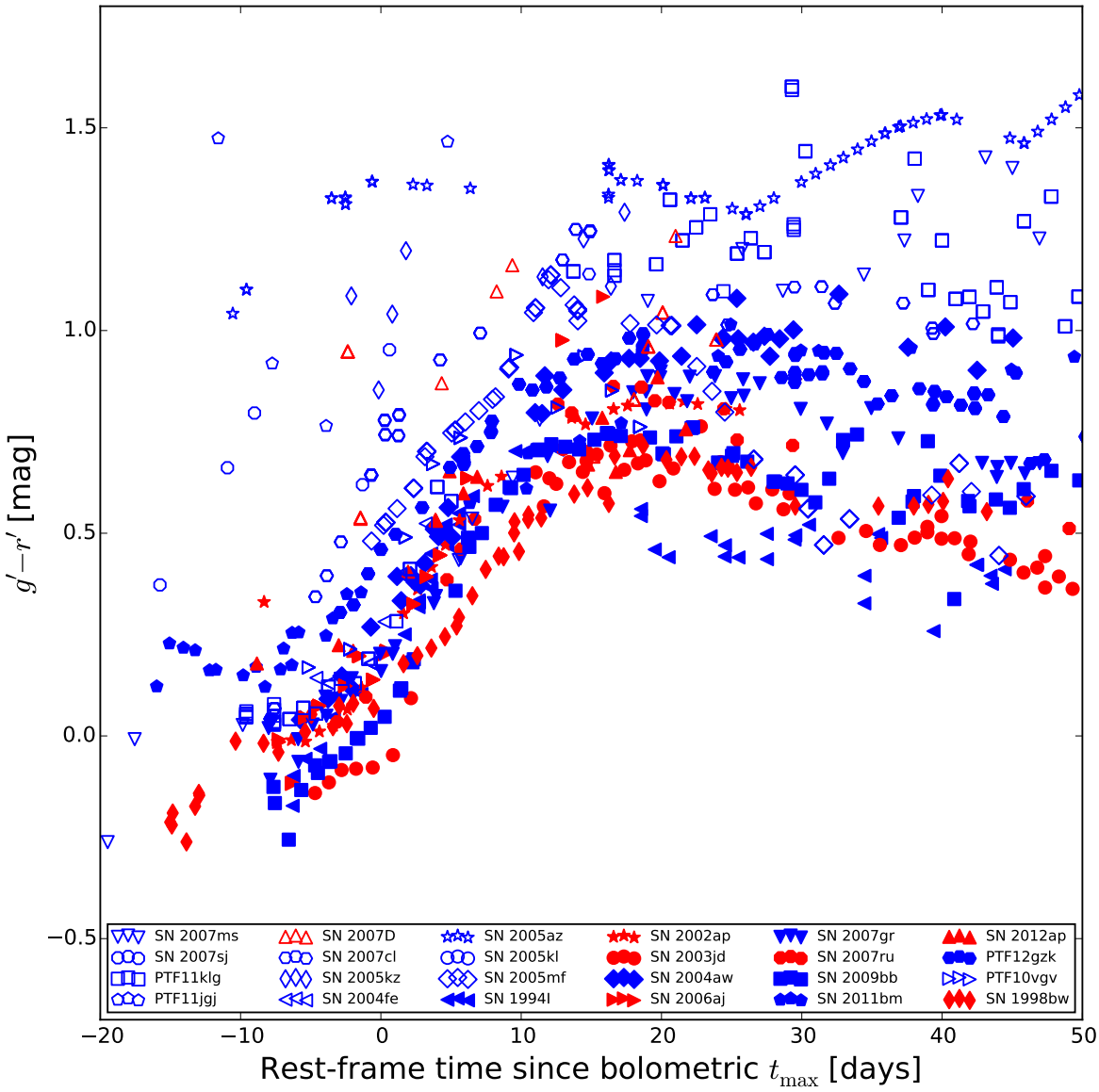

Figure 24. $g' - r'$ colour of the SNe Ic in the sample at $z < 0.05$. Open markers indicate SNe where $E(B-V)_{\rm host}$ is not known.

now (e.g., Gal-Yam et al. 2013). However, telescope time and funding are of limited supply; thus, the sample of SNe is affected in numerous ways. For example, many of the SNe are objects of interest; they display some unusual property that makes them targets for follow-up observations when they are spectroscopically confirmed, or they are nearby and bright. This is especially true of GRB-SNe and XRF-SNe, which are discovered only as a result of the detection of the high-energy transient event with which they are associated. Consequently, GRB-SNe and XRF-SNe are found at much greater distances that other SE-SNe and in different host environments. Some SNe are serendipitous discoveries in surveys designed for research in other areas, typically searches for SNe Ia, so unless the SE-SN is an object of interest it is not monitored. Furthermore, if a SE-SN is discovered as a result of a targeted survey in which particular galaxy types are observed at regular intervals because they display a propensity for SNe, then we will miss events that occur in less optimal environments. The cost of observing transients over numerous bands has resulted in an increase of single-band observations of SNe. If spectra are available it may be possible to estimate the bolometric properties of the the SN

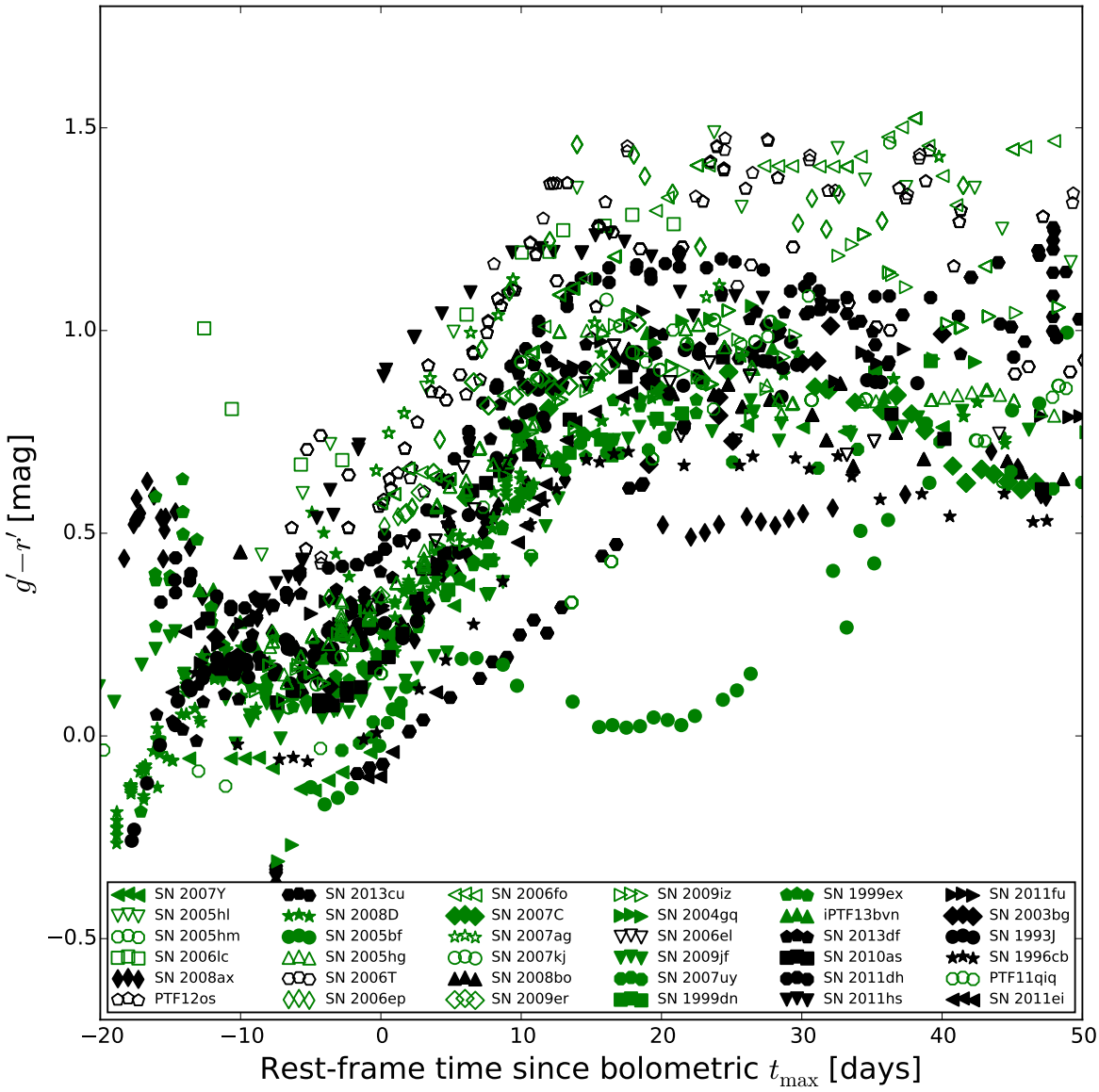

Figure 25. $g' - r'$ colour of the SNe Ib and SNe IIb in the sample at $z < 0.05$. Open markers indicate SNe where $E(B-V)_{\rm host}$ is not known.

by assuming its evolution is the same as that of a SN with a similar spectrum. Finally, observations favour SNe in less dusty regions of the host galaxy and those that are intrinsically luminous because their apparent brightness is greater. This leads to sampling of a larger comoving volume for more luminous SNe (Malmquist bias).

There are several consequences for our study. First, the luminosity functions are effectively luminosity functions for $z < 0.1$ because only the GRB-SNe and some SNe Ic-BL are sampled at higher redshifts. Second, the luminosity functions themselves may be overestimating the median luminosity if the nondetection of low-luminosity SNe is a significant issue. This is unquantifiable because rates of intrinsically dim SNe are unknown; however, a low-luminosity, nearby SN would be an object of interest (provided this is not a consequence of reddening). Our study shows that there appears to be a clear reduction in the number of SNe with $\log(L_{\rm p}) \lesssim 41.7$, yet there are clearly well-sampled SNe significantly below this luminosity. Given that the majority of these SNe are found at low redshift, and so would be observable at these luminosities, it appears that we are not missing intrinsically dim SNe in large numbers in the comoving volume we are

Table 9. Bolometric corrections derived from single-band photometry.

Band	Mean BC (mag)	σ (mag)	N
B	0.19	0.27	40
g'	−0.058	0.33	12
V	−0.34	0.21	40
r'	−0.43	0.28	27
R	−0.45	0.13	25
i'	−0.38	0.29	27
I	−0.51	0.18	24

Table 10. Median values for the fully bolometric sample.

SN Type	log(Lp)	$M_{\rm Ni}$ ($M_\odot$)
Ic-BL/GRB-SNe	$43.00\pm^{0.21}_{0.21}$	$0.34\pm^{0.13}_{0.19}$
Ic	$42.51\pm^{0.06}_{0.36}$	$0.16\pm^{0.03}_{0.10}$
Ib	$42.50\pm^{0.10}_{0.20}$	$0.14\pm^{0.04}_{0.04}$
IIb	$42.36\pm^{0.26}_{0.11}$	$0.11\pm^{0.04}_{0.04}$

typically sampling. It must also be considered that we do see SNe with relatively low ejecta and nickel masses; for example, SN 1994I was found to have $M_{\rm ej} < 1 M_\odot$ (Iwamoto et al. 1994), while SN 2007Y synthesised just $0.051 M_\odot$ of ^{56}Ni. This raises interesting questions of the SN mechanism and whether there is a lower limit on ejecta mass and nickel synthesis. Finally, we consider the effect of peculiar objects on our sample. This is generally minimised because peculiar objects (e.g., SN 2003bg, Mazzali et al. 2009; PTF12gzk, Ben-Ami et al. 2012; SN 2011bm, Valenti et al. 2012) do not constitute a significant proportion of each subtype, and if there are enough of them they become subtypes in their own right (e.g., SNe Ic-BL, GRB-SNe). We note that a good example of observational bias toward interesting objects is seen with the number of GRB-SNe that could be included in this study. We have 10 GRB-SNe that fulfil the criteria for inclusion, and this represents a significant fraction of those discovered.

10.2 Explosion characteristics

The median population statistics and relevant 1σ uncertainties for the fully bolometric sample are given in Table 10. As per Table 5, a hierarchy of peak luminosities is evident, with SNe Ic-BL/GRB-SNe generally more luminous than the SN Ic, IIb, and Ib populations. In terms of $M_{\rm Ni}$, we find that most types of SNe synthesise similar amounts of ^{56}Ni with the exception of the broad-lined SNe Ic, where the median value for $M_{\rm Ni}$ is more than double that of the others. Additionally, the median $t_{-1/2}$ is found to be shorter for these SNe compared to their less-energetic cousins. The degeneracy between $M_{\rm ej}$ and $E_{\rm k}$ in Equation 6 means that without photospheric velocities, found from spectral modeling, it is not possible to tell whether the typically narrower light curves of the SNe Ic is a consequence of smaller ejecta masses, more energetic explosions, or some amount of ^{56}Ni in the outer ejecta. Ejecta with significant amounts of ^{56}Ni mixed into the outer layers will rise more quickly as the diffusion time for the photons emitted in these regions will be less than that emitted more centrally. The models of Arnett (1982) assume that all light-curve powering sources are located centrally; if ^{56}Ni is located further out, then this model will return less-accurate values for the light-curve parameters.

10.3 Photometry

The scatter of light-curve colours at peak is unsurprising; there is no homogeneous explosion mechanism for SE-SNe as there is for SNe Ia. The reason for the narrowing of the colour curves after ~ 10 days is harder to explain. Attempts have been made to use this as a way of deriving host-galaxy extinction (e.g., Drout et al. 2011; Taddia et al. 2015), but this method is sensitive to the underlying spectrum, K-corrections, the quality of the photometry, the colours used, and the type of SN. It may have most applicability for low-redshift SNe.

The SNe Ic-BL appear to have bolometric peak coincident with the SED peak to the blue side of V, comparable to SNe IIb which are known for their blue spectra. This cannot be accounted for in the scatter of the distribution, as it falls short of covering the effective wavelength of V. A thorough investigation of this result cannot be undertaken with photometry and will require the use of spectra.

11 CONCLUSIONS

We have taken 85 SE-SNe from the literature and used the available photometry to build a set of optical pseudobolometric light curves and optical/NIR bolometric light curves. By using the same method and the same cosmological model, the database is as self-consistent as possible. The photometry was corrected for Galactic and host-galaxy extinction where such information was available. We found that fewer than 50% of the SNe had known host extinction values, so we searched the literature for SNe Ib/c and SNe II with this information known. From these data a series of distributions was constructed, and the median host extinction for each SN type was found and used as an estimate to correct for reddening when deriving bulk statistics.

The light curves were then analysed to reveal the peak luminosity and various temporal properties which were used to investigate the characteristics of SE-SNe. The analysis revealed that $t_{-1/2}$ is very loosely correlated with $t_{+1/2}$ but showed significant scatter around this value. K-S tests of the cumulative distribution functions for the decay times of the SNe revealed that most were likely drawn from the same population with the exception of SNe Ic/Ic-BL and SNe Ic/IIb. However, the presence of the Type Ic SNe PTF11rka and 2011bm, which display broad light curves, and a relatively small sample size skew the SN Ic CDF. Conversely, it is found that the SNe Ib and IIb generally take longer to rise than the SN Ic population. Using the equations of Arnett (1982), we can estimate the mass to kinetic energy ratio of the ejecta, which is related to the rise time. These properties are degenerate and can only be fully determined

via spectral modeling; consequently, we make no comment on the size, mass, or structure of the progenitor star.

It was also found that, in the absence of a known explosion time, the rise time of a light curve could be estimated from $t_{-1/2}$. A comparison between the peak values of the *UBVRI* pseudobolometric light curves and *UBVRI*NIR light curves of those SNe having enough data to build both revealed that a tight correlation forms in the $L_{\mathrm{p},UBVRI}$–$L_{\mathrm{p},UBVRI\mathrm{NIR}}$ parameter space that is independent of SN type, allowing the conversion of one value to the other. These relationships were then used to produce bolometric statistics for nearly all of the SN database.

It is shown that SNe Ic-BL and GRB-SNe occupy the upper part of the SE-SN luminosity function, with SNe IIb at the bottom. SNe Ic and SNe Ib show similar median peak luminosities. Using an approximation of "Arnett's law," the amount of ^{56}Ni synthesised in the core collapse of the stars that eventually go on to form the SN Ic-BL population is on average twice that of SNe Ic, Ib, and IIb. This is partly driven by the fact that all GRB-SNe are broad-lined and luminous.

The colour curves of the multiband photometry in the sample were analysed. The peak magnitude, time to peak, $t_{-1/2}$, and $t_{+1/2}$ were calculated for each band and compared with those of the bolometric light curve. To determine the colour curves and the colour at maximum, for each SN *BgVRr* photometry was converted to g' and r' where necessary. Our results confirm that there is evidence of a narrowing in the spread of $g'-r'$ for SNe with Milky Way and host-galaxy extinction corrections applied at ~ 10 days past bolometric maximum, though there is still a large range of possible values in this region. It is shown that the approximate wavelength of temporally coincident peaks between the multiband photometry and the bolometric LC occurs around the peak of the V band ($\lambda_{\mathrm{eff}} = 5505$ Å) for all but GRB-SNe, which are blueward of this. The photometry allowed us to investigate the possibility of using single-band observations and a BC to derive the bolometric parameters. The smallest spread in values was found for the R and I bands, but this was not replicated with i', which has an effective wavelength between these two Johnsons-Cousins filters. The uncertainties involved would lead to poorly constrained luminosities; thus, we reject the notion of using a single band as a proxy for the bolometric light curve at peak.

The importance of knowing the host-galaxy extinction cannot be understated. The peak luminosity of a SN, and all of the subsequent characteristics derived from that, depend on knowing this property. As such, we suggest that future work involving SE-SNe place a high priority on calculating or estimating the extinction at the source. This could be done through medium/high-resolution spectra and analysis of the Na I D absorption lines, via some method involving the colour evolution, or preferably both. If the colour method is used it is imperative that K-corrections are included. It is appreciated that these methods are not without their problems, however, and further analysis of the extinction in the environments of SE-SNe is needed.

Finally, each subtype presented here suffers from small-number statistics; hence, we identify the need for well-sampled SE-SN follow-up observations, particularly in volume-limited surveys, in order to improve the statistics and enhance our understanding of the evolutionary paths of massive stars.

12 APPENDIX

ACKNOWLEDGEMENTS

This research used resources of the National Energy Research Scientific Computing Center, a DOE Office of Science User Facility supported by the Office of Science of the U.S. Department of Energy under Contract No. DE-AC02-05CH11231. A.V.F.'s research was funded by NSF grant AST-1211916, the TABASGO Foundation, and the Christopher R. Redlich Fund. A.G.Y. is supported by the EU/FP7 via ERC grant no. 307260, "The Quantum Universe" I-Core program by the Israeli Committee for planning and budgeting and the ISF; by Minerva and ISF grants; by the Weizmann-UK âĂIJmaking connectionsâĂİ program; and by Kimmel and YeS awards.

References

Anupama G. C., Sahu D. K., Deng J., Nomoto K., Tominaga N., Tanaka M., Mazzali P. A., Prabhu T. P., 2005, ApJ, 631, L125
Arcavi I., et al., 2011, ApJ, 742, L18
Arnett W. D., 1982, ApJ, 253, 785
Ben-Ami S., et al., 2012, ApJ, 760, L33
Benetti S., et al., 2011, MNRAS, 411, 2726
Bessell M. S., Castelli F., Plez B., 1998, A&A, 333, 231
Bianco F. B., et al., 2014, ApJS, 213, 19
Bufano F., et al., 2012, ApJ, 753, 67
Bufano F., et al., 2014, MNRAS, 439, 1807
Cano Z., 2013, MNRAS, 434, 1098
Cano Z., et al., 2014, A&A, 568, A19
Cardelli J. A., Clayton G. C., Mathis J. S., 1989, ApJ, 345, 245
Clocchiatti A., Wheeler J. C., 1997, ApJ, 491, 375
Clocchiatti A., Suntzeff N. B., Covarrubias R., Candia P., 2011, AJ, 141, 163
Corsi A., et al., 2012, ApJ, 747, L5
D'Elia V., et al., 2015, A&A, 577, A116
Deng J., Tominaga N., Mazzali P. A., Maeda K., Nomoto K., 2005, ApJ, 624, 898
Drout M. R., et al., 2011, ApJ, 741, 97
Drout M. R., et al., 2015, preprint, (arXiv:1507.02694)
Eldridge J. J., Fraser M., Smartt S. J., Maund J. R., Crockett R. M., 2013, MNRAS, 436, 774
Filippenko A. V., 1988, AJ, 96, 1941
Filippenko A. V., 1997, ARA&A, 35, 309
Filippenko A. V., Matheson T., Ho L. C., 1993, ApJ, 415, L103
Folatelli G., et al., 2006, ApJ, 641, 1039
Folatelli G., Bersten M. C., Kuncarayakti H., Olivares Estay F., Anderson J. P., Holmbo S., Maeda K., Morrell N., 2014, ApJ, 792, 7
Foley R. J., et al., 2003, PASP, 115, 1220
Fremling C., et al., 2014, A&A, 565, A114
Fukugita M., Shimasaku K., Ichikawa T., 1995, PASP, 107, 945
Gal-Yam A., Ofek E. O., Shemmer O., 2002, MNRAS, 332, L73
Gal-Yam A., Mazzali P. A., Manulis I., Bishop D., 2013, PASP, 125, 749
Gal-Yam A., et al., 2014, Nature, 509, 471
Galama T. J., et al., 1998, Nature, 395, 670
Graham J. F., Fruchter A. S., 2013, ApJ, 774, 119
Greiner J., et al., 2015, Nature, 523, 189
Hamuy M., et al., 2009, ApJ, 703, 1612
Hjorth J., et al., 2003, Nature, 423, 847

Hunter D. J., et al., 2009, A&A, 508, 371
Iwamoto K., Nomoto K., Höflich P., Yamaoka H., Kumagai S., Shigeyama T., 1994, ApJ, 437, L115
Iwamoto K., et al., 1998, Nature, 395, 672
Jordi K., Grebel E. K., Ammon K., 2006, A&A, 460, 339
Kocevski D., et al., 2007, ApJ, 663, 1180
Kumar B., et al., 2013, MNRAS, 431, 308
Law N. M., et al., 2009, PASP, 121, 1395
Li W., et al., 2011, MNRAS, 412, 1441
Lyman J. D., Bersier D., James P. A., 2014, MNRAS, 437, 3848
Lyman J. D., Bersier D., James P. A., Mazzali P. A., Eldridge J. J., Fraser M., Pian E., 2016, MNRAS, 457, 328
Maeda K., et al., 2007, ApJ, 666, 1069
Marion G. H., et al., 2014, ApJ, 781, 69
Matheson T., Filippenko A. V., Ho L. C., Barth A. J., Leonard D. C., 2000, AJ, 120, 1499
Matheson T., Filippenko A. V., Li W., Leonard D. C., Shields J. C., 2001, AJ, 121, 1648
Matheson T., et al., 2003, ApJ, 599, 394
Mazzali P. A., 2000, A&A, 363, 705
Mazzali P. A., Lucy L. B., 1993, A&A, 279, 447
Mazzali P. A., Iwamoto K., Nomoto K., 2000, ApJ, 545, 407
Mazzali P. A., et al., 2002, ApJ, 572, L61
Mazzali P. A., et al., 2005, Science, 308, 1284
Mazzali P. A., et al., 2008, Science, 321, 1185
Mazzali P. A., Deng J., Hamuy M., Nomoto K., 2009, ApJ, 703, 1624
Melandri A., et al., 2012, A&A, 547, A82
Melandri A., et al., 2014, A&A, 567, A29
Milisavljevic D., et al., 2013, ApJ, 767, 71
Milisavljevic D., et al., 2015, ApJ, 799, 51
Mirabal N., Halpern J. P., An D., Thorstensen J. R., Terndrup D. M., 2006, ApJ, 643, L99
Modjaz M., et al., 2008, AJ, 135, 1136
Modjaz M., et al., 2009, ApJ, 702, 226
Morales-Garoffolo A., et al., 2014, MNRAS, 445, 1647
Nomoto K., Suzuki T., Shigeyama T., Kumagai S., Yamaoka H., Saio H., 1993, Nature, 364, 507
Pastorello A., et al., 2008, MNRAS, 389, 955
Patat F., et al., 2001, ApJ, 555, 900
Phillips M. M., 1993, ApJ, 413, L105
Pian E., et al., 2006, Nature, 442, 1011
Pignata G., et al., 2011, ApJ, 728, 14
Poznanski D., Prochaska J. X., Bloom J. S., 2012, MNRAS, 426, 1465
Pritchard T. A., Roming P. W. A., Brown P. J., Bayless A. J., Frey L. H., 2014, ApJ, 787, 157
Qiu Y., Li W., Qiao Q., Hu J., 1999, AJ, 117, 736
Richardson D., 2009, AJ, 137, 347
Richardson D., Branch D., Baron E., 2006, AJ, 131, 2233
Richmond M. W., Treffers R. R., Filippenko A. V., Paik Y., Leibundgut B., Schulman E., Cox C. V., 1994, AJ, 107, 1022
Richmond M. W., et al., 1996, AJ, 111, 327
Roy R., et al., 2013, MNRAS, 434, 2032
Sahu D. K., Tanaka M., Anupama G. C., Gurugubelli U. K., Nomoto K., 2009, ApJ, 697, 676
Sako M., et al., 2014, preprint, (arXiv:1401.3317)
Smartt S. J., 2009, ARA&A, 47, 63
Smith N., Owocki S. P., 2006, ApJ, 645, L45
Soderberg A. M., et al., 2008, Nature, 453, 469
Srivastav S., Anupama G. C., Sahu D. K., 2014, MNRAS, 445, 1932
Stritzinger M., Leibundgut B., 2005, A&A, 431, 423
Stritzinger M., et al., 2002, AJ, 124, 2100
Stritzinger M., et al., 2009, ApJ, 696, 713
Taddia F., et al., 2015, A&A, 574, A60
Taubenberger S., et al., 2006, MNRAS, 371, 1459
Taubenberger S., et al., 2011, MNRAS, 413, 2140
Tominaga N., et al., 2005, ApJ, 633, L97
Tomita H., et al., 2006, ApJ, 644, 400
Turatto M., et al., 2000, ApJ, 534, L57
Valenti S., et al., 2008, MNRAS, 383, 1485
Valenti S., et al., 2011, MNRAS, 416, 3138
Valenti S., et al., 2012, ApJ, 749, L28
Van Dyk S. D., et al., 2014, AJ, 147, 37
Wheeler J. C., Johnson V., Clocchiatti A., 2015, MNRAS, 450, 1295
Woosley S. E., Eastman R. G., Weaver T. A., Pinto P. A., 1994, ApJ, 429, 300
Yaron O., Gal-Yam A., 2012, PASP, 124, 668

APPENDIX A: HOST-GALAXY EXTINCTION

We searched the literature for core-collapse SNe with defined host-galaxy extinction in order to determine the distribution for the sample as a whole or individually. In addition to the SNe used in Table 1, we have also included SNe from Cano (2013), Pritchard et al. (2014), Cano et al. (2014), Richardson (2009), Richardson et al. (2006), and other individual SNe from the literature which failed the criteria described in Section 2.1. We also include all SNe II on the basis that, while the evolution of these objects may be different from that of SE-SNe, their position in the host is likely to be similar given their lifetimes (i.e., in star-forming regions). The total number used was 110.

A0.1 K-S tests

We performed K-S tests on the sample on a type-by-type basis. If the K-S test revealed that the distribution was drawn from the same population by having $P > 0.05$, then the populations were combined. SNe IIP and SNe IIL were combined into a single population owing to their small numbers. The interplay between the populations means that combining similar datasets is a risky task. For example, the SN IIb versus SN Ib K-S test returns $P = 0.055$, which is on the edge of the 5σ limit, yet SN IIb against SN Ic returns $P = 0.38$, and SN Ic against SN Ib returns $P = 0.487$; thus, populations were combined together only if the chance of the two being drawn from the same distribution was greater than 40% for all permutations of the individuals within the group. This limit is high but necessary to reduce the risk in combining datasets into a larger group that may have a low P value between some of its constituents.

The clear outlier is the distribution given by GRB-SNe, where K-S tests give $P < 0.05$ for every population. This does not imply that GRB-SN hosts are different from those of other SNe; the distribution of extinction values can be explained as a combination of distance and the luminosity function of SNe. We find that GRB-SNe, while more luminous on average than other SN types, are still limited to $L_{\rm peak} \approx 10^{43}$ erg s^{-1} in bolometric luminosity and are typically observed at redshifts much greater than other SNe. As a result, the sample is biased in two ways. First, these SNe are observed at larger distances because we recover them from GRBs; without this added high-energy component few, if any, of these SNe would be seen. Second, the limiting luminosity and distance mean that only the least-attenuated SN light will be observed, so if a GRB exploded in a dusty environment and had a corresponding SN, we would not see it

Table A1. Reddening [$E(B-V)$, mag] statistics of the populations.

SN Population	N	median	mean
IIP, IIL, II, IIb, IIn	25	$0.081\ ^{+0.1298}_{-0.026}$	0.130
Ib	22	$0.2235\ ^{+0.305}_{-0.157}$	0.30
Ic, Ic-BL	27	$0.174\ ^{+0.187}_{-0.116}$	0.244
GRB-SN	22	$0.0325\ ^{+0.00635}_{-0.024}$	0.040

as it would be below current detection limits. Furthermore, if we consider the entire sample, the non-Gaussian nature of all the distributions may be expected but their observed shape is determined by similar constraints. The probability that a SN is detected is reduced for higher local extinctions and lower intrinsic luminosities because these lower its apparent brightness. Hence, the distribution is more likely to show SNe with low host extinction, which in turn biases the result in favour of SNe in "clean" environments.

Thus, we return four populations:

- SNe IIP, IIL, II, IIb
- SNe Ib
- SNe Ic, Ic-BL
- GRB-SNe.

The median, upper and lower 34%, mean, and standard deviation for each population are given in Table A1. The discrepancy in median and mean is caused by the non-Gaussian distribution, so we use the median extinction as a typical extinction for SNe of that type and the upper and lower 34% as the 1σ boundaries. This median extinction and associated uncertainty is then applied to any SN without determined host extinction. For an individual SN such a correction could be deemed to be misleading; however, for a large dataset with several SNe utilising this method, we rely on "regression to the mean" — that is, for each SN where the extinction is underestimated, there will be a corresponding SN with extinction overestimated, and the uncertainties in this range provide a balance in terms of numbers centred on the average (the median in this case). The cumulative distributions are shown in Figure A1.

To test the accuracy of using this method, we take the SNe from the database with known host-galaxy extinction (SNe Ic/Ic-BL/GRB-SNe = 15, SNe Ib/IIb = 22) and apply the median extinction correction when constructing the bolometric light curve. This is then compared with the case when no host extinction correction is applied and when the actual extinction is applied. The results are shown in Figure A3 for the application of median host extinction, Figure A2 for the actual values, and Figure A4 for no correction. It is apparent that the character of the luminosity function changes when median $E(B-V)_{\rm host}$ is used in place of the literature value; this is to be expected around the extremes of the distribution because no SN is being corrected for a large host extinction but all are being corrected. The statistics returned in Table A2 show that the mean and median of the luminosity functions remain similar, giving confidence in the conversion method to return bulk statistics. However, in the absence of $E(B-V)_{\rm host}$ the statistics returned are

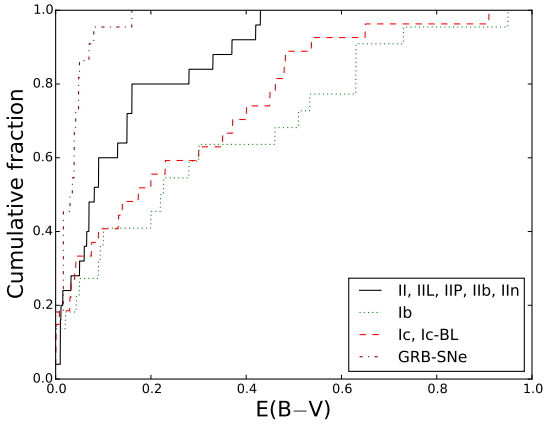

Figure A1. Cumulative distribution of reddening values for SNe sorted by population.

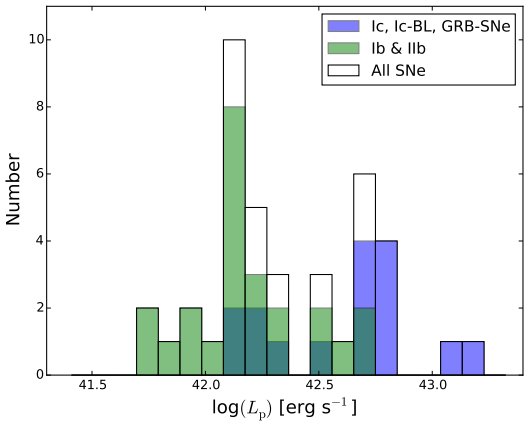

Figure A2. *BVRI* luminosity function for SNe with their host extinction correction applied using the values given in the literature. Colours are as described in Figure 9.

generally lower than the corrected values; again, this would be expected as they represent a lower limit. It is interesting to note that the SN Ic median values are very similar for no extinction and the known $E(B-V)_{\rm host}$, although this is not reflected in the mean value.

APPENDIX B: TABLES

This paper has been typeset from a TEX/LATEX file prepared by the author.

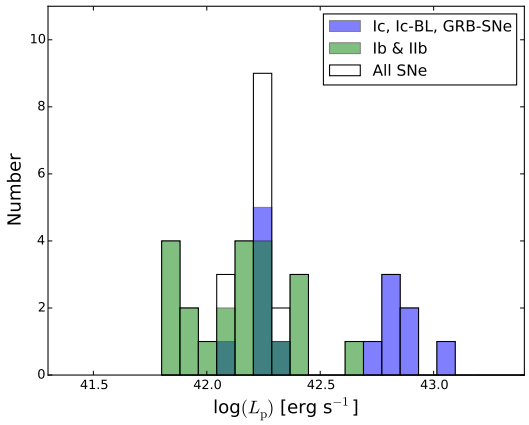

Figure A3. *BVRI* luminosity function of the same SNe as in Figure A2 but with a type-dependent host extinction correction applied. Colours are as described in Figure 9.

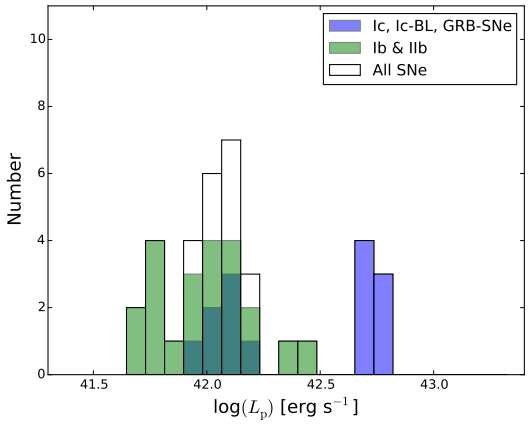

Figure A4. *BVRI* luminosity function of the same SNe as in Figure A2 but with no host extinction correction applied. Colours are as described in Figure 9.

Table A2. Host extinction tests on peak-luminosity statistics.

Literature extinction values			
SN Type	median	mean	σ
All Ic	42.69	42.59	0.32
Ib/IIb	42.15	42.17	0.24
bulk	42.23	42.34	0.34
Median extinction values			
SN Type	median	mean	σ
All Ic	42.72	42.61	0.38
Ib/IIb	42.17	42.15	0.23
bulk	42.24	42.34	0.38
No extinction correction			
SN Type	median	mean	σ
All Ic	42.67	42.47	0.4
Ib/IIb	42.01	41.99	0.2
bulk	42.11	42.12	0.38

Table B1. *BVRI* pseudobolometric light curve statistics.

SN	Type	log(Lp)	$M_{\rm Ni}$ ($M_\odot$)	$t_{\rm p}$ (days)	$t_{-1/2}$ (days)	$t_{+1/2}$ (days)	Width (days)
1993J	IIb	$42.231\pm^{0.068}_{0.066}$	$0.087\pm^{0.015}_{0.012}$	19.148±0.033	10.313±0.017	12.808±0.116	23.121±0.118
1994I	Ic	$42.271\pm^{0.346}_{0.328}$	$0.064\pm^{0.080}_{0.034}$	12.252±0.211	5.541±0.137	8.522±0.509	14.063±0.527
1996cb	IIb	$41.871\pm^{0.123}_{0.123}$	$0.034\pm^{0.015}_{0.011}$	16.993±1.650	10.737±0.000	15.444±0.017	26.181±0.017
1998bw	GRB-SN	$42.780\pm^{0.031}_{0.023}$	$0.260\pm^{0.022}_{0.016}$	15.861±0.177	9.734±0.372	15.858±0.779	25.593±0.863
1999dn	Ib	$42.134\pm^{0.084}_{0.061}$	$0.052\pm^{0.023}_{0.015}$	13.916±2.841	-	21.827±3.638	-
1999ex	Ib	$42.335\pm^{0.082}_{0.082}$	$0.106\pm^{0.022}_{0.019}$	18.349±0.036	9.226±0.053	15.958±0.606	25.183±0.608
2002ap	Ic-BL	$42.217\pm^{0.010}_{0.006}$	$0.060\pm^{0.001}_{0.001}$	13.011±0.000	6.466±0.060	15.506±0.165	21.972±0.175
2003bg	IIb	$42.226\pm^{0.027}_{0.014}$	$0.076\pm^{0.012}_{0.009}$	16.624±1.656	10.504±0.146	28.374±1.318	38.878±1.326
2003jd	Ic-BL	$42.795\pm^{0.090}_{0.089}$	$0.219\pm^{0.054}_{0.042}$	12.504±0.179	9.372±0.505	14.067±0.317	23.439±0.596
2004aw	Ic	$42.448\pm^{0.030}_{0.044}$	-	-	-	21.273±1.340	-
2004fe*	Ic	$42.152\pm^{0.031}_{0.030}$	$0.057\pm^{0.010}_{0.009}$	14.680±1.653	9.276±0.101	-	-
2004gq	Ib	$42.087\pm^{0.010}_{0.006}$	-	-	-	18.582±0.465	-
2005az*	Ic	$41.981\pm^{0.013}_{0.015}$	-	-	-	27.282±0.146	-
2005bf	Ib	$42.170\pm^{0.025}_{0.023}$	$0.073\pm^{0.006}_{0.005}$	18.325±0.351	-	-	-
2005hg*	Ib	$42.233\pm^{0.010}_{0.013}$	-	-	-	17.943±0.237	-
2005hl*	Ib	$41.993\pm^{0.008}_{0.005}$	-	-	-	21.656±0.667	-
2005hm*	Ib	$41.958\pm^{-0.013}_{0.041}$	$0.048\pm^{0.002}_{0.008}$	19.927±1.669	12.591±0.250	14.682±1.455	27.274±1.476
2005kl*	Ic	$41.485\pm^{0.008}_{0.008}$	-	-	-	20.115±0.027	-
2005kr*	Ic-BL	$42.759\pm^{0.072}_{0.038}$	$0.187\pm^{0.059}_{0.035}$	11.405±1.669	7.207±0.252	-	-
2005ks*	Ic-BL	$42.291\pm^{0.066}_{0.078}$	$0.068\pm^{0.020}_{0.017}$	12.368±1.656	7.815±0.142	-	-
2005kz*	Ic	$42.004\pm^{0.034}_{0.031}$	-	-	-	-	-
2005mf*	Ic	$42.121\pm^{0.033}_{0.024}$	-	-	-	17.281±0.493	-
2006T*	IIb	$42.145\pm^{0.011}_{0.011}$	$0.054\pm^{0.007}_{0.007}$	14.148±1.651	8.940±0.051	14.433±0.031	23.372±0.059
2006aj	GRB-SN	$42.685\pm^{0.020}_{0.019}$	$0.138\pm^{0.007}_{0.006}$	9.587±0.040	6.779±0.155	-	-
2006el*	IIb	$42.041\pm^{0.024}_{0.016}$	-	-	-	15.594±0.660	-
2006ep*	Ib	$41.942\pm^{0.012}_{0.013}$	$0.042\pm^{0.005}_{0.005}$	18.002±1.653	11.375±0.101	15.034±0.013	26.409±0.102
2006fe*	Ic	$42.263\pm^{0.025}_{0.026}$	$0.079\pm^{0.013}_{0.012}$	15.830±1.711	10.002±0.455	19.197±1.431	29.199±1.502
2006fo*	Ib	$42.164\pm^{0.019}_{0.019}$	-	-	-	19.017±0.124	-
14475*	Ic-BL	$42.558\pm^{0.047}_{0.048}$	$0.110\pm^{0.029}_{0.024}$	10.501±1.760	6.635±0.613	18.037±1.403	24.672±1.531
2006jo*	Ib	$42.371\pm^{0.020}_{0.020}$	$0.071\pm^{0.013}_{0.011}$	10.366±1.651	6.550±0.067	10.081±0.472	16.630±0.476
2006lc*	Ib	$41.954\pm^{0.005}_{0.008}$	$0.034\pm^{0.004}_{0.004}$	13.837±1.651	8.743±0.050	14.036±0.050	22.779±0.071
2006nx*	Ic-BL	$42.847\pm^{0.051}_{0.021}$	$0.276\pm^{0.067}_{0.040}$	14.279±1.698	9.022±0.401	-	-
2007C	Ib	$42.588\pm^{0.085}_{0.084}$	-	-	-	12.373±0.186	-
2007D*	Ic-BL	$42.121\pm^{0.085}_{0.082}$	-	-	-	-	-
2007Y	Ib	$41.750\pm^{0.064}_{0.072}$	$0.028\pm^{0.005}_{0.005}$	18.757±0.350	9.284±0.569	15.327±0.285	24.610±0.636
2007ag*	Ib	$41.884\pm^{0.015}_{0.014}$	-	-	-	20.052±0.673	-
2007cl*	Ic	$42.077\pm^{0.010}_{0.010}$	-	-	-	15.616±0.259	-
2007gr	Ic	$42.087\pm^{0.042}_{0.043}$	$0.045\pm^{0.005}_{0.005}$	13.146±0.229	8.530±0.025	15.270±0.081	23.800±0.085
2007kj*	Ib	$42.017\pm^{0.009}_{0.008}$	-	-	-	-	-
2007ms*	Ic	$42.319\pm^{0.008}_{0.017}$	$0.122\pm^{0.011}_{0.013}$	22.231±1.666	14.047±0.231	24.625±0.434	38.672±0.491

Table B1 – *continued BVRI* pseudobolometric light curve statistics.

SN	Type	log(Lp)	$M_{\rm Ni}$ ($M_\odot$)	$t_{\rm p}$ (days)	$t_{-1/2}$ (days)	$t_{+1/2}$ (days)	Width (days)
2007nc*	Ib	$42.065\pm^{0.064}_{0.016}$	$0.055\pm^{0.015}_{0.007}$	17.734±1.800	11.205±0.718	19.059±4.382	30.264±4.440
2007qv*	Ic	$42.514\pm^{0.023}_{0.022}$	-	-	-	-	-
2007qx*	Ic	$42.118\pm^{0.197}_{0.041}$	$0.054\pm^{0.045}_{0.013}$	15.094±2.758	9.537±2.211	-	-
2007ru	Ic-BL	$42.810\pm^{0.038}_{0.009}$	$0.194\pm^{0.018}_{0.005}$	10.242±0.047	-	14.640±0.485	-
2007sj*	Ic	$41.961\pm^{0.022}_{0.021}$	$0.036\pm^{0.006}_{0.005}$	14.542±1.658	9.188±0.164	-	-
2007uy	Ib	$42.675\pm^{0.270}_{0.260}$	$0.241\pm^{0.214}_{0.110}$	19.075±0.284	-	15.360±1.160	-
2008D	Ib	$42.125\pm^{0.252}_{0.240}$	$0.069\pm^{0.055}_{0.030}$	19.293±0.229	13.239±0.194	17.042±0.722	30.281±0.747
2008ax	IIb	$42.099\pm^{0.025}_{0.024}$	$0.065\pm^{0.004}_{0.004}$	19.283±0.127	10.144±0.085	15.279±0.318	25.423±0.329
2008bo	IIb	$41.757\pm^{0.011}_{0.011}$	-	-	-	9.240±0.010	-
2008hw	GRB-SN	$43.156\pm^{0.050}_{0.050}$	$0.496\pm^{0.064}_{0.057}$	12.307±0.100	-	-	-
2009bb	Ic	$42.685\pm^{0.123}_{0.121}$	$0.171\pm^{0.057}_{0.042}$	12.631±0.095	6.637±0.059	13.060±0.357	19.697±0.362
2009er*	Ib	$42.724\pm^{0.013}_{0.012}$	-	-	-	14.225±0.049	-
2009iz*	Ib	$42.085\pm^{0.010}_{0.010}$	$0.070\pm^{0.006}_{0.006}$	21.828±1.650	13.793±0.000	23.220±0.169	37.013±0.169
2009jf	Ib	$42.478\pm^{0.022}_{0.027}$	$0.169\pm^{0.010}_{0.011}$	21.267±0.164	11.212±0.444	19.901±0.631	31.113±0.771
2010as	IIb	$42.524\pm^{0.088}_{0.087}$	$0.117\pm^{0.027}_{0.022}$	12.442±0.122	9.661±0.024	16.541±0.415	26.202±0.415
2010bh	GRB-SN	$42.365\pm^{0.053}_{0.053}$	$0.082\pm^{0.011}_{0.010}$	12.737±0.099	3.287±0.303	9.286±0.884	12.573±0.934
2010ma	GRB-SN	$43.060\pm^{0.234}_{0.071}$	$0.346\pm^{0.444}_{0.136}$	10.331±4.338	-	12.450±0.482	-
2011bm	Ic	$42.705\pm^{0.031}_{0.037}$	$0.427\pm^{0.033}_{0.036}$	34.586±0.151	-	43.446±1.544	-
2011dh	IIb	$42.084\pm^{0.008}_{0.012}$	$0.052\pm^{0.001}_{0.001}$	15.712±0.017	9.638±0.034	14.525±0.119	24.163±0.124
2011ei	IIb	$41.969\pm^{0.089}_{0.088}$	$0.044\pm^{0.010}_{0.008}$	17.732±0.033	10.247±0.033	16.893±0.360	27.140±0.362
2011fu	IIb	$42.338\pm^{0.008}_{0.012}$	-	-	-	18.016±0.283	-
2011hs	IIb	$41.903\pm^{0.011}_{0.012}$	$0.021\pm^{0.001}_{0.001}$	8.588±0.057	7.718±0.023	11.199±0.263	18.917±0.264
2011kl[a]	GRB-SN	$43.324\pm^{0.166}_{0.157}$	-	15.169±0.071	6.889±0.142	12.712±0.355	19.601±0.382
2012ap	Ic-BL	$42.472\pm^{0.162}_{0.158}$	$0.109\pm^{0.052}_{0.035}$	13.192±0.308	8.648±1.337	15.546±0.174	24.193±1.348
2012bz	GRB-SN	$42.795\pm^{0.029}_{0.032}$	$0.240\pm^{0.026}_{0.013}$	13.491±0.224	9.838±0.066	17.110±0.177	26.947±0.189
2013cq	GRB-SN	$42.960\pm^{0.050}_{0.100}$	-	-	-	-	-
2013cu	IIb	$42.661\pm^{0.007}_{0.006}$	$0.125\pm^{0.003}_{0.002}$	9.009±0.082	6.890±0.031	12.516±0.163	19.406±0.166
2013df	IIb	$42.198\pm^{0.034}_{0.037}$	$0.091\pm^{0.008}_{0.008}$	21.793±0.103	13.897±0.101	11.727±0.310	25.624±0.326
2013dx	GRB-SN	$42.831\pm^{0.027}_{0.032}$	-	-	11.697±1.768	14.389±0.841	26.086±1.958
2013ge	Ibc	$42.132\pm^{0.019}_{0.024}$	$0.068\pm^{0.009}_{0.009}$	18.878±1.697	11.928±0.395	19.953±0.285	31.881±0.487
PTF09dh/2009dr*	Ic-BL	$42.892\pm^{0.035}_{0.03}$	-	-	-	18.546±0.247	-
PTF10gvb*	Ic-BL	$42.775\pm^{0.067}_{0.067}$	-	-	18.179±19.629	14.344±0.483	32.522±19.635
PTF10inj*	Ib	$42.438\pm^{0.157}_{0.143}$	-	-	-	36.035±0.490	-
PTF10qif*	Ib	$42.455\pm^{0.123}_{0.118}$	-	-	-	13.452±1.764	-
PTF10vgv*	Ic	$42.493\pm^{0.065}_{0.063}$	$0.094\pm^{0.029}_{0.022}$	10.347±1.687	6.538±0.354	9.969±0.000	16.507±0.354
PTF11bli*	Ibc	$42.071\pm^{0.018}_{0.018}$	$0.065\pm^{0.008}_{0.007}$	20.627±1.658	13.033±0.164	-	-
PTF11jgj*	Ic	$42.088\pm^{0.022}_{0.018}$	$0.072\pm^{0.010}_{0.009}$	22.072±2.170	13.947±1.409	-	-
PTF11klg*	Ic	$42.105\pm^{0.144}_{0.125}$	$0.057\pm^{0.030}_{0.018}$	16.393±1.678	10.358±0.303	14.530±0.039	24.887±0.306
PTF11qiq*	Ib	$42.161\pm^{0.500}_{0.010}$	-	-	-	17.000±1.000	-
PTF11rka*	Ic	$42.723\pm^{0.050}_{0.045}$	-	-	-	45.781±3.909	-

Table B1 – *continued BVRI* pseudobolometric light curve statistics.

PTF12gzk	Ic	$42.708\pm^{0.031}_{0.029}$	$0.226\pm^{0.023}_{0.020}$	16.345±0.455	-	23.643±0.065	-
PTF12os*	IIb	$41.409\pm^{0.007}_{0.010}$	-	-	-	17.095±0.492	-
iPTF13bvn	Ib	$41.997\pm^{0.012}_{0.011}$	$0.043\pm^{0.001}_{0.001}$	15.953±0.098	8.990±0.024	13.582±0.098	22.572±0.101
iPTF14dby*	Ic-BL	$42.373\pm^{0.043}_{0.042}$	$0.140\pm^{0.025}_{0.022}$	22.462±1.678	14.193±0.303	20.615±0.884	34.808±0.934

* SN has not been corrected for host extinction. $L_{\rm p}$ and $M_{\rm Ni}$ values are lower limits

[a]SN 2011kl was primarily powered by a magnetar. The mass of ^{56}Ni synthesised in the explosion was negligible (Greiner et al. 2015)

Table B2. *UBVRI*NIR pseudobolometric light curve statistics.

SN	Type	log(Lp)	$M_{\rm Ni}$ ($M_\odot$)	$t_{\rm p}$ (days)	$t_{-1/2}$ (days)	$t_{+1/2}$ (days)	Width (days)
1998bw	GRB-SN	$42.953\pm^{0.042}_{0.026}$	$0.386\pm^{0.043}_{0.026}$	15.861±0.177	9.445±0.607	14.639±0.894	24.084±1.081
1999dn	Ib	$42.360\pm^{0.191}_{0.163}$	$0.088\pm^{0.073}_{0.038}$	13.916±2.841	-	19.790±4.210	-
2002ap	Ic-BL	$42.373\pm^{0.018}_{0.008}$	$0.086\pm^{0.004}_{0.002}$	13.011±0.000	6.076±0.130	13.629±0.362	19.705±0.384
2003dh	GRB-SN	$42.94\pm^{0.08}_{0.09}$	$0.308\pm^{0.102}_{0.083}$	12.65±1.66	-	15.845±0.590	-
2005bf	Ib	$42.385\pm^{0.033}_{0.032}$	$0.119\pm^{0.012}_{0.010}$	18.325±0.351	-	-	-
2005hg*	Ib	$42.377\pm^{0.029}_{0.027}$	-	-	12.215±0.051	19.900±0.727	32.115±0.728
2005mf*	Ic	$42.255\pm^{0.095}_{0.051}$	-	-	-	18.696±0.899	-
2006aj	GRB-SN	$42.839\pm^{0.025}_{0.017}$	$0.197\pm^{0.012}_{0.008}$	9.587±0.040	6.227±0.526	11.059±4.141	17.285±4.175
2007Y	Ib	$41.963\pm^{0.065}_{0.099}$	$0.046\pm^{0.008}_{0.010}$	18.757±0.350	7.406±0.916	11.507±0.916	18.912±1.295
2007gr	Ic	$42.258\pm^{0.061}_{0.059}$	$0.066\pm^{0.011}_{0.009}$	13.146±0.229	7.951±0.051	14.300±0.067	22.251±0.084
2007uy	Ib	$42.846\pm^{0.360}_{0.318}$	$0.358\pm^{0.474}_{0.188}$	19.075±0.284	-	12.944±1.512	-
2008D	Ib	$42.292\pm^{0.355}_{0.305}$	$0.101\pm^{0.130}_{0.051}$	19.293±0.229	13.697±0.106	16.897±0.606	30.594±0.615
2008ax	IIb	$42.284\pm^{0.037}_{0.036}$	$0.099\pm^{0.009}_{0.008}$	19.283±0.127	9.259±0.243	13.262±0.526	22.522±0.579
2009iz*	Ib	$42.200\pm^{0.028}_{0.024}$	$0.091\pm^{0.014}_{0.012}$	21.750±1.936	12.959±0.278	25.824±0.893	38.782±0.936
2009jf	Ib	$42.640\pm^{0.034}_{0.036}$	$0.246\pm^{0.022}_{0.021}$	21.267±0.164	10.633±0.652	18.821±0.285	29.453±0.711
2011bm	Ic	$42.880\pm^{0.058}_{0.049}$	$0.638\pm^{0.094}_{0.070}$	34.586±0.151	-	43.461±1.449	-
2011dh	IIb	$42.205\pm^{0.019}_{0.016}$	$0.068\pm^{0.003}_{0.003}$	15.712±0.017	9.837±0.075	13.346±0.045	23.182±0.087
2011hs	IIb	$42.027\pm^{0.017}_{0.018}$	$0.028\pm^{0.001}_{0.001}$	8.588±0.057	8.303±0.000	12.072±0.227	20.375±0.227

* SN has not been corrected for host extinction. $L_{\rm p}$ and $M_{\rm Ni}$ values are lower limits

Table B3. Parameters derived from the fully bolometric $L_{\rm p}$ values.

SN	Type	log (Lp)	$t_{\rm p}$ (days)	$M_{\rm Ni}$ ($M_\odot$)
1993J	IIb	$42.456\pm^{0.109}_{0.088}$	19.148±0.033	$0.146\pm^{0.042}_{0.027}$
1994I	Ic	$42.473\pm^{0.409}_{0.363}$	12.252±0.211	$0.102\pm^{0.164}_{0.059}$
1996cb	IIb	$42.082\pm^{0.179}_{0.163}$	16.993±1.650	$0.055\pm^{0.036}_{0.021}$
1998bw	GRB-SN	$43.061\pm^{0.080}_{0.046}$	15.861±0.177	$0.496\pm^{0.091}_{0.047}$
1999dn	Ib	$42.402\pm^{0.229}_{0.183}$	13.916±2.841	$0.097\pm^{0.097}_{0.044}$
1999ex	Ib	$42.544\pm^{0.124}_{0.105}$	18.349±0.036	$0.172\pm^{0.058}_{0.037}$
2002ap	Ic-BL	$42.415\pm^{0.055}_{0.028}$	13.011±0.000	$0.094\pm^{0.013}_{0.006}$
2003bg	IIb	$42.424\pm^{0.086}_{0.058}$	16.624±1.656	$0.119\pm^{0.040}_{0.024}$
2003dh	GRB-SN	$42.981\pm^{0.116}_{0.107}$	12.65±1.66	$0.339\pm^{0.153}_{0.102}$
2003jd	Ic-BL	$42.988\pm^{0.134}_{0.115}$	12.504±0.179	$0.341\pm^{0.128}_{0.082}$
2004aw	Ic	$42.659\pm^{0.063}_{0.056}$	-	-
2004fe*	Ic	$42.354\pm^{0.099}_{0.083}$	14.680±1.653	$0.091\pm^{0.035}_{0.023}$
2004gq	Ib	$42.388\pm^{0.046}_{0.028}$	-	-
2005az*	Ic	$42.173\pm^{0.086}_{0.070}$	-	-
2005bf	Ib	$42.426\pm^{0.071}_{0.052}$	18.325±0.351	$0.131\pm^{0.026}_{0.017}$
2005hg*	Ib	$42.418\pm^{0.067}_{0.047}$	-	-
2005hl*	Ib	$42.167\pm^{0.060}_{0.027}$	-	-
2005hm*	Ib	$42.237\pm^{0.073}_{0.093}$	19.927±1.669	$0.092\pm^{0.025}_{0.023}$
2005kl*	Ic	$41.979\pm^{0.080}_{0.064}$	-	-
2005kr*	Ic-BL	$43.006\pm^{0.117}_{0.057}$	11.405±1.669	$0.330\pm^{0.153}_{0.073}$
2005ks*	Ic-BL	$42.440\pm^{0.107}_{0.087}$	12.368±1.656	$0.096\pm^{0.040}_{0.026}$
2005kz*	Ic	$42.212\pm^{0.101}_{0.084}$	-	-
2005mf*	Ic	$42.296\pm^{0.133}_{0.071}$	-	-
2006T*	IIb	$42.322\pm^{0.054}_{0.036}$	14.148±1.651	$0.082\pm^{0.020}_{0.014}$
2006aj	GRB-SN	$42.880\pm^{0.062}_{0.038}$	9.587±0.040	$0.217\pm^{0.034}_{0.019}$
2006el*	IIb	$42.237\pm^{0.086}_{0.063}$	-	-
2006ep*	Ib	$42.142\pm^{0.075}_{0.060}$	18.002±1.653	$0.067\pm^{0.019}_{0.014}$
2006fe*	Ic	$42.533\pm^{0.094}_{0.081}$	15.830±1.711	$0.147\pm^{0.053}_{0.037}$
2006fo*	Ib	$42.372\pm^{0.099}_{0.080}$	-	-
14475*	Ic-BL	$42.753\pm^{0.108}_{0.092}$	10.501±1.760	$0.173\pm^{0.077}_{0.050}$
2006jo*	Ib	$42.542\pm^{0.086}_{0.052}$	10.366±1.651	$0.105\pm^{0.039}_{0.023}$
2006lc*	Ib	$42.130\pm^{0.044}_{0.030}$	13.837±1.651	$0.051\pm^{0.011}_{0.008}$
2006nx*	Ic-BL	$43.032\pm^{0.111}_{0.066}$	14.279±1.698	$0.422\pm^{0.181}_{0.097}$
2007C	Ib	$42.749\pm^{0.155}_{0.136}$	-	-
2007D*	Ic-BL	$42.282\pm^{0.156}_{0.135}$	-	-
2007Y	Ib	$42.005\pm^{0.103}_{0.119}$	18.757±0.350	$0.051\pm^{0.015}_{0.013}$
2007ag*	Ib	$42.085\pm^{0.078}_{0.061}$	-	-
2007cl*	Ic	$42.282\pm^{0.078}_{0.064}$	-	-
2007gr	Ic	$42.299\pm^{0.099}_{0.079}$	13.146±0.229	$0.073\pm^{0.020}_{0.013}$
2007kj*	Ib	$42.214\pm^{0.072}_{0.055}$	-	-
2007ms*	Ic	$42.556\pm^{0.052}_{0.041}$	22.231±1.666	$0.211\pm^{0.043}_{0.032}$

Table B3 – *continued* Parameters derived from the fully bolometric $L_{\rm p}$ values.

SN	Type	log(Lp)	$t_{\rm p}$ (days)	$M_{\rm Ni}$ ($M_\odot$)
2007nc*	Ib	$42.260\pm^{0.125}_{0.063}$	17.734±1.800	$0.087\pm^{0.040}_{0.019}$
2007qv*	Ic	$42.783\pm^{0.062}_{0.043}$	-	-
2007qx*	Ic	$42.337\pm^{0.207}_{0.069}$	15.094±2.758	$0.090\pm^{0.078}_{0.025}$
2007ru	Ic-BL	$43.033\pm^{0.054}_{0.032}$	10.242±0.047	$0.323\pm^{0.044}_{0.024}$
2007sj*	Ic	$42.152\pm^{0.074}_{0.052}$	14.542±1.658	$0.057\pm^{0.017}_{0.011}$
2007uy	Ib	$42.887\pm^{0.398}_{0.338}$	19.075±0.284	$0.394\pm^{0.604}_{0.215}$
2008D	Ib	$42.333\pm^{0.393}_{0.325}$	19.293±0.229	$0.111\pm^{0.167}_{0.059}$
2008ax	IIb	$42.326\pm^{0.075}_{0.056}$	19.283±0.127	$0.109\pm^{0.021}_{0.014}$
2008bo	IIb	$41.972\pm^{0.071}_{0.055}$	-	-
2008hw	GRB-SN	$43.337\pm^{0.095}_{0.078}$	12.307±0.100	$0.751\pm^{0.190}_{0.127}$
2009bb	Ic	$42.863\pm^{0.162}_{0.143}$	12.631±0.095	$0.258\pm^{0.119}_{0.073}$
2009er*	Ib	$42.916\pm^{0.089}_{0.072}$	-	-
2009iz*	Ib	$42.241\pm^{0.066}_{0.044}$	21.828±1.650	$0.101\pm^{0.024}_{0.016}$
2009jf	Ib	$42.682\pm^{0.072}_{0.057}$	21.267±0.164	$0.271\pm^{0.051}_{0.035}$
2010as	IIb	$42.689\pm^{0.158}_{0.139}$	12.442±0.122	$0.171\pm^{0.077}_{0.048}$
2010bh	GRB-SN	$42.600\pm^{0.168}_{0.113}$	12.737±0.099	$0.142\pm^{0.068}_{0.033}$
2010ma	GRB-SN	$43.244\pm^{0.272}_{0.098}$	10.331±4.338	$0.529\pm^{0.789}_{0.227}$
2011bm	Ic	$42.922\pm^{0.096}_{0.069}$	34.586±0.151	$0.702\pm^{0.176}_{0.106}$
2011dh	IIb	$42.246\pm^{0.057}_{0.036}$	15.712±0.017	$0.075\pm^{0.011}_{0.006}$
2011ei	IIb	$42.177\pm^{0.146}_{0.129}$	17.732±0.033	$0.072\pm^{0.029}_{0.018}$
2011fu	IIb	$42.538\pm^{0.045}_{0.034}$	-	-
2011hs	IIb	$42.068\pm^{0.055}_{0.038}$	8.588±0.057	$0.031\pm^{0.004}_{0.003}$
2011kl[a]	GRB-SN	$43.529\pm^{0.174}_{0.148}$	15.169±0.071	-
2012ap	Ic-BL	$42.676\pm^{0.203}_{0.182}$	13.192±0.308	$0.174\pm^{0.109}_{0.062}$
2012bz	GRB-SN	$43.005\pm^{0.100}_{0.052}$	13.491±0.224	$0.378\pm^{0.105}_{0.048}$
2013cq	GRB-SN	$43.186\pm^{0.086}_{0.117}$	13.000±2.000	$0.555\pm^{0.211}_{0.184}$
2013cu	IIb	$42.843\pm^{0.067}_{0.050}$	9.009±0.082	$0.191\pm^{0.033}_{0.022}$
2013df	IIb	$42.397\pm^{0.074}_{0.058}$	21.793±0.103	$0.144\pm^{0.028}_{0.019}$
2013dx	GRB-SN	$42.962\pm^{0.225}_{0.077}$	12.261±5.484	$0.316\pm^{0.417}_{0.139}$
2013ge	Ibc	$42.335\pm^{0.077}_{0.064}$	18.878±1.697	$0.109\pm^{0.032}_{0.023}$
PTF09dh/2009dr*	Ic-BL	$43.082\pm^{0.078}_{0.059}$	-	-
PTF10inj*	Ib	$42.620\pm^{0.215}_{0.186}$	-	-
PTF10qif*	Ib	$42.636\pm^{0.182}_{0.162}$	-	-
PTF10vgv*	Ic	$42.682\pm^{0.132}_{0.115}$	10.347±1.687	$0.145\pm^{0.076}_{0.047}$
PTF11bli*	Ibc	$42.266\pm^{0.081}_{0.065}$	20.627±1.658	$0.101\pm^{0.030}_{0.021}$
PTF11jgj*	Ic	$42.293\pm^{0.090}_{0.072}$	22.072±2.170	$0.114\pm^{0.039}_{0.026}$
PTF11klg*	Ic	$42.309\pm^{0.208}_{0.175}$	16.393±1.678	$0.090\pm^{0.069}_{0.036}$
PTF11qiq*	Ib	$42.352\pm^{0.545}_{0.057}$	-	-
PTF11rka*	Ic	$42.905\pm^{0.117}_{0.097}$	-	-

Table B3 – *continued* Parameters derived from the fully bolometric $L_{\rm p}$ values.

SN	Type	log(Lp)	$t_{\rm p}$ (days)	$M_{\rm Ni}$ ($M_\odot$)
PTF12gzk	Ic	$42.904\pm^{0.077}_{0.058}$	16.345±0.455	$0.355\pm^{0.079}_{0.052}$
PTF12os*	IIb	$41.588\pm^{0.047}_{0.030}$	-	-
iPTF13bvn	Ib	$42.211\pm^{0.067}_{0.037}$	15.953±0.098	$0.070\pm^{0.012}_{0.006}$
iPTF14dby*	Ic-BL	$42.575\pm^{0.104}_{0.087}$	22.462±1.678	$0.223\pm^{0.079}_{0.053}$

* SN has not been corrected for host extinction. $L_{\rm p}$ and $M_{\rm Ni}$ values are lower limits

[a]SN 2011kl was primarily powered by a magnetar. The mass of ^{56}Ni synthesised in the explosion was negligible (Greiner et al. 2015)

Table B4. $M_{\rm ej}^3/E_{\rm k}$ values for the sample at different opacities.

SN	Type	$\frac{M_{\rm ej}^3}{[{\rm M}_\odot]}/\frac{E_{\rm k}}{[10^{51}{\rm erg}]}$ $\kappa = 0.05$ g cm^{-2}	$\frac{M_{\rm ej}^3}{[{\rm M}_\odot]}/\frac{E_{\rm k}}{[10^{51}{\rm erg}]}$ $\kappa = 0.07$ g cm^{-2}	$\frac{M_{\rm ej}^3}{[{\rm M}_\odot]}/\frac{E_{\rm k}}{[10^{51}{\rm erg}]}$ $\kappa = 0.1$ g cm^{-2}
14475	Ic-BL	$0.567\pm^{0.487}_{0.295}$	$0.289\pm^{0.248}_{0.150}$	$0.142\pm^{0.122}_{0.074}$
1993J	IIb	$6.267\pm^{0.044}_{0.043}$	$3.198\pm^{0.022}_{0.022}$	$1.567\pm^{0.011}_{0.011}$
1994I	Ic	$1.051\pm^{0.074}_{0.071}$	$0.536\pm^{0.038}_{0.036}$	$0.263\pm^{0.019}_{0.018}$
1996cb	IIb	$3.888\pm^{1.745}_{1.304}$	$1.984\pm^{0.890}_{0.665}$	$0.972\pm^{0.436}_{0.326}$
1998bw	GRB-SN	$2.951\pm^{0.134}_{0.130}$	$1.506\pm^{0.068}_{0.066}$	$0.738\pm^{0.033}_{0.032}$
1999dn	Ib	$1.749\pm^{1.928}_{1.047}$	$0.892\pm^{0.984}_{0.534}$	$0.437\pm^{0.482}_{0.262}$
1999ex	Ib	$5.286\pm^{0.041}_{0.041}$	$2.697\pm^{0.021}_{0.021}$	$1.321\pm^{0.010}_{0.010}$
2002ap	Ic-BL	$1.336\pm^{0.000}_{0.000}$	$0.682\pm^{0.000}_{0.000}$	$0.334\pm^{0.000}_{0.000}$
2003bg	IIb	$3.561\pm^{1.646}_{1.221}$	$1.817\pm^{0.840}_{0.623}$	$0.890\pm^{0.411}_{0.305}$
2003jd	Ic-BL	$1.140\pm^{0.067}_{0.064}$	$0.582\pm^{0.034}_{0.033}$	$0.285\pm^{0.017}_{0.016}$
2004fe	Ic	$2.165\pm^{1.153}_{0.823}$	$1.105\pm^{0.588}_{0.420}$	$0.541\pm^{0.288}_{0.206}$
2005bf	Ib	$5.257\pm^{0.415}_{0.392}$	$2.682\pm^{0.212}_{0.200}$	$1.314\pm^{0.104}_{0.098}$
2005hm	Ib	$7.352\pm^{2.790}_{2.170}$	$3.751\pm^{1.423}_{1.107}$	$1.838\pm^{0.697}_{0.543}$
2005kr	Ic-BL	$0.789\pm^{0.573}_{0.370}$	$0.403\pm^{0.293}_{0.189}$	$0.197\pm^{0.143}_{0.092}$
2005ks	Ic-BL	$1.091\pm^{0.713}_{0.477}$	$0.557\pm^{0.364}_{0.243}$	$0.273\pm^{0.178}_{0.119}$
2006T	IIb	$1.868\pm^{1.037}_{0.731}$	$0.953\pm^{0.529}_{0.373}$	$0.467\pm^{0.259}_{0.183}$
2006aj	GRB-SN	$0.394\pm^{0.007}_{0.007}$	$0.201\pm^{0.003}_{0.003}$	$0.098\pm^{0.002}_{0.002}$
2006ep	Ib	$4.896\pm^{2.062}_{1.566}$	$2.498\pm^{1.052}_{0.799}$	$1.224\pm^{0.515}_{0.391}$
2006fe	Ic	$2.928\pm^{1.487}_{1.075}$	$1.494\pm^{0.759}_{0.549}$	$0.732\pm^{0.372}_{0.269}$
2006jo	Ib	$0.538\pm^{0.434}_{0.269}$	$0.275\pm^{0.221}_{0.137}$	$0.135\pm^{0.109}_{0.067}$
2006lc	Ib	$1.709\pm^{0.974}_{0.681}$	$0.872\pm^{0.497}_{0.347}$	$0.427\pm^{0.243}_{0.170}$
2006nx	Ic-BL	$1.938\pm^{1.100}_{0.770}$	$0.989\pm^{0.561}_{0.393}$	$0.485\pm^{0.275}_{0.193}$
2007Y	Ib	$5.771\pm^{0.443}_{0.419}$	$2.945\pm^{0.226}_{0.214}$	$1.443\pm^{0.111}_{0.105}$
2007gr	Ic	$1.393\pm^{0.100}_{0.094}$	$0.711\pm^{0.051}_{0.048}$	$0.348\pm^{0.025}_{0.024}$
2007ms	Ic	$11.388\pm^{3.817}_{3.049}$	$5.810\pm^{1.948}_{1.556}$	$2.847\pm^{0.954}_{0.762}$
2007nc	Ib	$4.611\pm^{2.176}_{1.606}$	$2.353\pm^{1.110}_{0.819}$	$1.153\pm^{0.544}_{0.401}$
2007qx	Ic	$2.420\pm^{2.316}_{1.341}$	$1.235\pm^{1.182}_{0.684}$	$0.605\pm^{0.579}_{0.335}$
2007ru	Ic-BL	$0.513\pm^{0.010}_{0.009}$	$0.262\pm^{0.005}_{0.005}$	$0.128\pm^{0.002}_{0.002}$
2007sj	Ic	$2.085\pm^{1.126}_{0.800}$	$1.064\pm^{0.575}_{0.408}$	$0.521\pm^{0.282}_{0.200}$
2007uy	Ib	$6.173\pm^{0.377}_{0.360}$	$3.149\pm^{0.192}_{0.184}$	$1.543\pm^{0.094}_{0.090}$
2008D	Ib	$6.460\pm^{0.312}_{0.301}$	$3.296\pm^{0.159}_{0.154}$	$1.615\pm^{0.078}_{0.075}$
2008ax	IIb	$6.447\pm^{0.172}_{0.169}$	$3.289\pm^{0.088}_{0.086}$	$1.612\pm^{0.043}_{0.042}$
2008hw	GRB-SN	$1.070\pm^{0.035}_{0.034}$	$0.546\pm^{0.018}_{0.018}$	$0.267\pm^{0.009}_{0.009}$
2009bb	Ic	$1.187\pm^{0.036}_{0.035}$	$0.606\pm^{0.018}_{0.018}$	$0.297\pm^{0.009}_{0.009}$
2009iz	Ib	$10.585\pm^{3.582}_{2.856}$	$5.401\pm^{1.828}_{1.457}$	$2.646\pm^{0.896}_{0.714}$
2009jf	Ib	$9.537\pm^{0.297}_{0.290}$	$4.866\pm^{0.151}_{0.148}$	$2.384\pm^{0.074}_{0.072}$
2010as	IIb	$1.117\pm^{0.044}_{0.043}$	$0.570\pm^{0.023}_{0.022}$	$0.279\pm^{0.011}_{0.011}$
2010bh	GRB-SN	$1.227\pm^{0.039}_{0.038}$	$0.626\pm^{0.020}_{0.019}$	$0.307\pm^{0.010}_{0.009}$

Table B4 – *continued* $M_{\rm ej}^3/E_{\rm k}$ values for the sample at different opacities.

SN	Type	$\frac{M_{\rm ej}^3}{[{\rm M}_\odot]}/\frac{E_{\rm k}}{[10^{51}{\rm erg}]}$ $\kappa = 0.05$ g cm^{-2}	$\frac{M_{\rm ej}^3}{[{\rm M}_\odot]}/\frac{E_{\rm k}}{[10^{51}{\rm erg}]}$ $\kappa = 0.07$ g cm^{-2}	$\frac{M_{\rm ej}^3}{[{\rm M}_\odot]}/\frac{E_{\rm k}}{[10^{51}{\rm erg}]}$ $\kappa = 0.1$ g cm^{-2}
2010ma	GRB-SN	$0.531\pm^{1.628}_{0.471}$	$0.271\pm^{0.830}_{0.240}$	$0.133\pm^{0.407}_{0.118}$
2011bm	Ic	$66.714\pm^{1.170}_{1.154}$	$34.038\pm^{0.597}_{0.589}$	$16.678\pm^{0.292}_{0.289}$
2011dh	IIb	$2.842\pm^{0.012}_{0.012}$	$1.450\pm^{0.006}_{0.006}$	$0.710\pm^{0.003}_{0.003}$
2011ei	IIb	$4.609\pm^{0.034}_{0.034}$	$2.352\pm^{0.017}_{0.017}$	$1.152\pm^{0.009}_{0.008}$
2011hs	IIb	$0.254\pm^{0.007}_{0.007}$	$0.129\pm^{0.003}_{0.003}$	$0.063\pm^{0.002}_{0.002}$
2011kl	GRB-SN	$2.468\pm^{0.047}_{0.046}$	$1.259\pm^{0.024}_{0.023}$	$0.617\pm^{0.012}_{0.011}$
2012ap	Ic-BL	$1.412\pm^{0.137}_{0.127}$	$0.720\pm^{0.070}_{0.065}$	$0.353\pm^{0.034}_{0.032}$
2012bz	GRB-SN	$1.544\pm^{0.105}_{0.100}$	$0.788\pm^{0.054}_{0.051}$	$0.386\pm^{0.026}_{0.025}$
2013cq	GRB-SN	$1.332\pm^{1.029}_{0.649}$	$0.679\pm^{0.525}_{0.331}$	$0.333\pm^{0.257}_{0.162}$
2013cu	IIb	$0.307\pm^{0.011}_{0.011}$	$0.157\pm^{0.006}_{0.006}$	$0.077\pm^{0.003}_{0.003}$
2013df	IIb	$10.517\pm^{0.201}_{0.198}$	$5.366\pm^{0.103}_{0.101}$	$2.629\pm^{0.050}_{0.050}$
2013dx	GRB-SN	$1.054\pm^{3.570}_{0.955}$	$0.538\pm^{1.821}_{0.487}$	$0.263\pm^{0.892}_{0.239}$
2013ge	Ibc	$5.921\pm^{2.433}_{1.858}$	$3.021\pm^{1.241}_{0.948}$	$1.480\pm^{0.608}_{0.465}$
PTF10vgv	Ic	$0.534\pm^{0.443}_{0.272}$	$0.273\pm^{0.226}_{0.139}$	$0.134\pm^{0.111}_{0.068}$
PTF11bli	Ibc	$8.440\pm^{3.059}_{2.404}$	$4.306\pm^{1.561}_{1.226}$	$2.110\pm^{0.765}_{0.601}$
PTF11jgj	Ic	$11.066\pm^{5.037}_{3.751}$	$5.646\pm^{2.570}_{1.914}$	$2.767\pm^{1.259}_{0.938}$
PTF11klg	Ic	$3.367\pm^{1.605}_{1.181}$	$1.718\pm^{0.819}_{0.602}$	$0.842\pm^{0.401}_{0.295}$
PTF12gzk	Ic	$3.328\pm^{0.387}_{0.356}$	$1.698\pm^{0.197}_{0.181}$	$0.832\pm^{0.097}_{0.089}$
iPTF13bvn	Ib	$3.020\pm^{0.075}_{0.073}$	$1.541\pm^{0.038}_{0.037}$	$0.755\pm^{0.019}_{0.018}$
iPTF14dby	Ic-BL	$11.869\pm^{3.963}_{3.168}$	$6.056\pm^{2.022}_{1.616}$	$2.967\pm^{0.991}_{0.792}$